

ENERGY TRANSFER IN Eu^{3+}

DOPED GLASSES

By

MICHAEL DEWAYNE FURLOUGH

Bachelor of Science

Dillard University

New Orleans, Louisiana

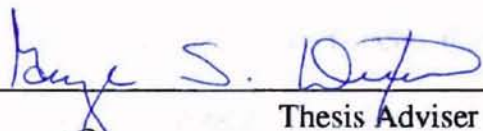
1992

Submitted to the Faculty of the
Graduate College of the
Oklahoma State University
in partial fulfillment of
the requirements for
the Degree of
MASTER OF SCIENCE
July, 1996

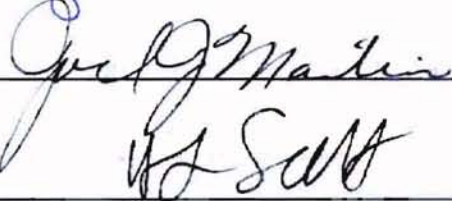
ENERGY TRANSFER IN Eu^{3+}


DOPED GLASSES

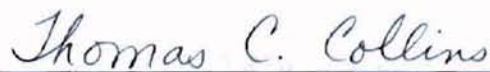
Thesis Approved:



Thesis Adviser







Dean of Graduate College

ACKNOWLEDGMENTS

I wish to express my heartfelt thanks to my research advisor and friend Dr. George S. Dixon. Without his assistance and patience, this thesis would not have been possible.

I would also like to express my thanks to Dr. Joel J. Martin's Laboratory. First, because it was Dr. Martin that recommended that I work for Dr. Dixon. Second, because of his helpful assistants, Dr. David Hart, Charles Hunt, and Michael Hamilton. Dr. Hart for being there for a young graduate student and easing the tension and stress with his unique sense of humor. Charles Hunt because without his assistance in the Crystal Growth Laboratory none of my samples could have been prepared for my research and also for his unique sense of humor too.

I would like to thank all my classmates Anne Georgalas, Sheena Jacob, Cindy Porter, Jeff McCullough, Steve Willoughby, John Snodgrass, Robert Wolf, Ricardo Nieves, Felicia Walker, Joy E. Ferris, and Jong Eul Lee. They made my experience at Oklahoma State University memorable.

Here is a special thank you to my mother, Mary C. Furlough, who has always stood behind me and told me that she BELIEVED in me. Special thanks to my sister, Zena V. Penn, and my brother, Kenneth W. Furlough, and also my dad, H. Furlough.

TABLE OF CONTENTS

Chapter		Page
I.	INTRODUCTION.....	1
	Amorphous Solids.....	3
	Continuous Random Network.....	4
	Glass Formers and Modifiers.....	6
	Phonon-Assisted Energy Transfer.....	7
	Results of Powell and Gang.....	9
	Statement of Purpose.....	10
II.	EXPERIMENTAL.....	17
	Samples.....	17
	Experimental Apparatus.....	19
	Experimental Procedures.....	21
III.	RESULTS AND DISCUSSION.....	26
	Current Model.....	26
	Spectral Structures.....	30
	Energy Transfer Characteristics.....	58
IV.	SUMMARY AND CONCLUSIONS.....	68
	REFERENCES.....	70

LIST OF TABLES

Table		Page
I.	Sample Compositions (mole %)	18
II.	Rising Edge Of The Boson Peaks	29
III.	Rising Edge of Low Frequency Boson Peaks and Onset of Secondary Peaks	33
IV.	Spectral Energy Transfer Time Constant	61

LIST OF FIGURES

Figure	Page
1. The two general cooling paths by which an assembly of atoms can condense into the solid state. Scenario 1 is the path to the crystalline state; scenario 2 is the rapid-quench path to the amorphous solid state.....	12
2. Two dimensional schematic of the structure of (a) crystalline SiO ₂ , (b) is a SiO ₂ glass, and (c) M ₂ O-SiO ₂ glass. The small solid circles are the silicon atoms, open circles the oxygen atoms, and the large shaded circles the alkali atoms.....	13
3. The relative orientation of two corner sharing tetrahedra in SiO ₂ , showing the short range order and one aspect of the intermediate range order. The Si atoms (dark) are surrounded tetrahedrally at distance r by four O atoms and each O atom bridges between two Si atoms with an angle θ that varies from site to site. This specifies the SRO. The dihedral angles δ , Δ , giving the angular orientation of tetrahedra about their bridging O-Si bonds, are defined in this paper as elements of IRO.....	14
4. Schematic representation of the formation of non-bridging oxygen in silicates on dissolution of alkali oxide.....	15
5. Schematic representation of a single-phonon-assisted energy transfer process.....	16
6. Site-selection spectroscopy using fluorescence line-narrowing experimental equipment diagram for the study of energy transfer in glasses doped with Eu ³⁺	24
7. Experimental arrangement and orientation of the glass sample.....	25

8. Raman spectra of glasses. All data were obtained at room temperature. The low frequency region of the boson peak is shown for all three members of this series of glasses. Curve A is the LiSiO glass; curve B is the Na-modified glass; curve D is the Rb-modified glass, while curve D and E are not used in this study.....34
9. Raman spectra of LiSiO glass. All data were obtained at room temperature. The low frequency region of the boson peak is shown for the LiSiO glass in this series of glasses. The inset is a full Raman spectrum of the LiSiO modified glass.....35
10. Raman spectra of Na glass. All data were obtained at room temperature. The low frequency region of the boson peak is shown for the Na glass in this series of glasses. The inset is a full Raman spectrum of the Na modified glass.....36
11. Raman spectra of Rb glass. All data were obtained at room temperature. The low frequency region of the boson peak is shown for the Rb glass in this series of glasses. The inset is a full Raman spectrum of the Rb modified glass.....37
12. Show the absorption spectra for LS glass over a spectrum range of 570 - 590 nm performed at room temperature on a Cary 05 spectrophotometer.....38
13. Shows the absorption spectra for LiSiO glass over a spectrum range of 570 - 590 nm performed at temperature on a Cary 05 spectrophotometer.....39
14. Show the absorption spectra for Na glass over a spectrum range of 570 - 590 nm performed at room temperature on a Cary 05 spectrophotometer.....40
15. Show the absorption spectra for Rb glass over a spectrum range of 570 - 590 nm performed at room temperature on a Cary 05 spectrophotometer.....41

Figure	Page
16. LS glass spectra obtained at an excitation wavelength of $\lambda_{ex} = 578$ nm. This series of graphs were taken at a temperature of 70 K and $T = 1.0, 3.0,$ and 5.0 ms.....	42
17. LS glass spectra obtained at an excitation wavelength of $\lambda_{ex} = 579$ nm. This series of graphs were taken at a temperature of 70 K and $T = 1.0, 3.0,$ and 5.0 ms.....	43
18. LS glass spectra obtained at an excitation wavelength of $\lambda_{ex} = 580$ nm. This series of graphs were taken at a temperature of 70 K $T = 1.0, 3.0,$ and 5.0 ms.....	44
19. LiSiO glass spectra obtained at an excitation wavelength of $\lambda_{ex} = 578$ nm. This series of graphs were taken at a temperature of 70 K and $T = 1.0, 3.0,$ and 5.0 ms.....	45
20. LiSiO glass spectra obtained at an excitation wavelength of $\lambda_{ex} = 579$ nm. This series of graphs were taken at a temperature of 70 K and $T = 1.0, 3.0,$ and 5.0 ms.....	46
21. LiSiO glass spectra obtained at an excitation wavelength of $\lambda_{ex} = 580$ nm. This series of graphs were taken at a temperature of 70 K and $T = 1.0, 3.0,$ and 5.0 ms.....	47
22. Na glass spectra obtained at an excitation wavelength of $\lambda_{ex} = 578$ nm. This series of graphs were taken at a temperature of 70 K and $T = 1.0, 3.0,$ and 5.0 ms.....	48
23. Na glass spectra obtained at an excitation wavelength of $\lambda_{ex} = 579$ nm. This series of graphs were taken at a temperature of 70 K and $T = 1.0, 3.0,$ and 5.0 ms.....	49
24. Na glass spectra obtained at an excitation wavelength of $\lambda_{ex} = 580$ nm. This series of graphs were taken at a temperature of 70 K and $T = 1.0, 3.0,$ and 5.0 ms.....	50
25. Rb glass spectra obtained at an excitation wavelength of $\lambda_{ex} = 578$ nm. This series of graphs were taken at a temperature of 70 K and $T = 1.0, 3.0,$ and 5.0 ms.....	51

Figure	Page
26. Rb glass spectra obtained at an excitation wavelength of $\lambda_{ex} = 579$ nm. This series of graphs were taken at a temperature of 70 K and $T = 1.0, 3.0,$ and 5.0 ms.....	52
27. Rb glass spectra obtained at an excitation wavelength of $\lambda_{ex} = 580$ nm. This series of graphs were taken at a temperature of 70 K and $T = 1.0, 3.0,$ and 5.0 ms.....	53
28. Plot of the onset of side peaks using their respective mobility edges as the scaling factor. The glasses are in this order LS, LiSiO, Na, and Rb with 578, 579 (anti-stokes), 579(stokes), and 580 nm respectively.....	54
29. Plot of the onset of side peaks normalized with respect to their lowest peak value. The glasses are in this order LS, LiSiO, Na, and Rb with 578, 579 (anti-stokes), 579(stokes), and 580 nm respectively.....	55
30. Spectral Peak Area vs. Time log plot for an excitation of 578 nm at 70 K, ranging from $T = 1.0, 3.0,$ and 5.0 ms for LS, LiSiO, Na, and Rb glasses. Demonstrating a constant decline in the area under the curve.....	56
31. Spectral Peak Area vs. Time log plot for an excitation of 579 nm at 70 K, ranging from $T = 1.0, 3.0,$ and 5.0 ms for LS, LiSiO, Na, and Rb glasses. Demonstrating a constant decline in the area under the curve.....	57
32. Spectral Peak Area vs. Time log plot for an excitation of 580 nm at 70 K, ranging from $T = 1.0, 3.0,$ and 5.0 ms for LS, LiSiO, Na, and Rb glasses. Demonstrating a constant decline in the area under the curve.....	61
33. Normalized Width vs. Time plot for an excitation of 578 nm at 70 K, ranging from $T = 1.0, 3.0,$ and 5.0 ms for LS, LiSiO, Na, and Rb glasses.....	62
34. Normalized Width vs. Time plot for an excitation of 579 nm at 70 K, ranging from $T = 1.0, 3.0,$ and 5.0 ms for LS, LiSiO, Na, and Rb glasses.....	63

35. Normalized Width vs. Time plot for an excitation of 580 nm at 70 K, ranging from $T= 1.0, 3.0,$ and 5.0 ms for LS, LiSiO, Na, and Rb glasses.....64
36. Spectral Energy Transfer Time plot for an excitation of 578 nm at 70 K, ranging from $T= 1.0, 3.0,$ and 5.0 ms for LS, LiSiO, Na, and Rb glasses.....65
37. Spectral Energy Transfer Time plot for an excitation of 579 nm at 70 K, ranging from $T= 1.0, 3.0,$ and 5.0 ms for LS, LiSiO, Na, and Rb glasses.....66
38. Spectral Energy Transfer Time plot for an excitation of 580 nm at 70 K, ranging from $T= 1.0, 3.0,$ and 5.0 ms for LS, LiSiO, Na, and Rb glasses.....67

CHAPTER I

INTRODUCTION

Glass lasers research increased tremendously during the seventies primarily as a possible solution to the world's energy shortage. This was because fusion research had a requirement for large neodymium glass lasers. Laser driven fusion is based on deuterium an inexhaustible fuel obtained from water. Glass lasers can be produced in one or two ways first by doping glass with rare-earth ions or two, by combining two or more rare-earth ions plus a transitional metal [1] . Rare-earth ions have been studied since the early seventies due to their optical properties in host glasses [2] . For instance, Nd^{3+} has been studied for its importance to laser applications. Europium has been studied because of its spectrum and transitions in local environments [3, 4] . Rare-earth ions have been studied particularly because of their potential usefulness in high power laser systems, and second, because of what can be discovered about the local structural properties of glass hosts [2, 3] .

In amorphous solids local strains and defects increase inhomogeneous broadening by $\approx 100 \text{ cm}^{-1}$, while for crystals they only give rise to linewidths $\approx 1.0 \text{ cm}^{-1}$ [5] . Site-selection excitation allows the study of optical processes at much greater resolution than the inhomogeneous broadening, so that even in glasses

resolution of 1.0 cm^{-1} or less is possible. This is accomplished by using an excitation source that is narrow compared to the inhomogeneous linewidth. In a site-selection experiment the spectral resolution is limited by the width of the narrow band source or the homogeneous linewidth, whichever is greater [5].

Inhomogeneous broadening is the result of the statistical distribution of ligand fields that optically active ions encounter in different sites in these glasses [6]. Homogeneous broadening can be defined as what one would see if all optically active ions were in the same site. Then the response of each individual atom in the system is equally and homogeneously broadened. This broadening can result from interaction of the ions with the phonons that modulate the ligand field at a given site or from lifetime broadening. An energy state is sharp only if the system stays in that state for some infinite amount of time. Otherwise, Heisenberg's [7] uncertainty principle defines the uncertain energy as:

$$\Delta E \Delta t \geq \frac{\hbar}{2}, \quad (1)$$

where $\Delta E = \hbar \Delta \omega$ and $2\Delta \omega = \Delta \omega_0$ is equal to full width at half maximum of the frequency distribution. This is where the lifetime broadening condition of

$$\Delta \omega_0 \tau \gg 1, \quad (2)$$

where $\Delta t = \tau$ and τ is the sum of both radiative and non-radiative lifetimes [5] .

First, this paper will talk about how amorphous solids and crystal are formed, followed by a discussion of the Zachariasen model [8, 9], continuous random network. Then a section on phonon-assisted energy transfer, followed by a brief section on glass formers and modifiers, will be presented. Finally, the related work of Powell and Gang [3] will be discussed.

Amorphous Solids

A glass is an amorphous solid formed from the melt. Any material can be prepared as an amorphous solid [10] . Amorphous and crystalline solids have two quite different solidification processes (see figure 1). The process leading to forming a crystalline solid happens at T_f (freezing temperature). Crystalline solids are usually arrived at by the use of very slow cooling rates. This is because crystalline centers must form first. On the other hand, amorphous solids are often arrived at through very high cooling rates [11] . Amorphous solids on the microscopic level are inherently disordered systems. Unlike crystals, each ion in an amorphous solid is in a unique environment.

Solidification of a crystalline solid is accompanied by a discontinuous volume change at the melting point [11] . But in a glass the volume change is smaller and occurs continuously over temperature region below T_g (glass transition temperature)

where the liquid-to-glass transition begins, where T_f (freezing temperature) is circumvented without trouble [11].

It can be seen in figure 2 that lack of translational symmetry is one of the obvious differences between glasses and crystals. Zallen [11] uses a picture of a gas to make his comparison. He uses the term randomness that is not an appropriate description of amorphous solids. The term randomness best describes the atomic positions of a gas viewed as point particles. The amorphous solid, however, demonstrates a high degree of local correlation. As seen in figure 2b, the amorphous solid has three nearest neighbors at approximately equal distances. Bond angles, represented here by dark lines, are also nearly equal when they meet at atomic positions. Both of these parameters (see figure 2a) are almost equal to those for crystals [11].

Continuous Random Network

The main structural difference between amorphous and crystalline solids is the absence of long-range order, which is mainly due to a strong disorder in the array of equilibrium atomic positions. This is exactly opposite of a crystal where long-range order is present. Crystals exhibit a translational periodic array when atoms are in equilibrium positions. The atomic-scale structures for amorphous solids are still unknown, but can be determined through diffraction experiments for crystals [11, 12].

Zachariasen [9] proposed that the local bonding in an amorphous solid is similar to its crystalline analog, but small variations in bond angles and, possibly, bond lengths destroy the periodic lattice while retaining a continuously bonded network. Zachariasen and Warren [9], through many different experiments, with the aid of x-ray diffraction contributed quantitative information about the Zachariasen model [8]. Warren and co-workers [7] clarification of radial distribution functions contributed two things to short range order (SRO) and one to intermediate range order (IRO). Local order around network former elements like Si, B, and P in oxide glasses are the main reasons for short range order. Most of these bonds are strongly covalent directional bonds, like the tetrahedral bonds [8, 9].

A brief discussion of the Zachariasen model [9] will aid in the discussion of amorphous solids. The Zachariasen model [9] includes four components of SRO. The first consists of only Si-O bonds with similar lengths, r , which means the sample has global range order (GRO). Silicon is considered to be four coordinated to oxygen, because silicon is tetrahedrally bonded to four oxygen atoms. Oxygen, on the other hand, is only two coordinated, because it only bridges between two silicon atoms. Zachariasen [9] also states that the Si-O-Si angles, θ , (see figure 3) are broadly distributed, which is the source of noncrystallinity in amorphous solids. There is only one component of IRO present and no edge-sharing or facing-sharing tetrahedra, therefore no two-rings [8, 9].

After Warren and co-workers [9] conducted x-diffraction experiments to test the new model, the Zachariasen-Warren model [9], it became known as the 'continuous random network' (CRN) [8, 9]. This CRN model added a few new components to existing model. The first component was to the range of the radius (r) is actually narrower, approximately $r = 1.61 \text{ \AA}$ (see figure 3) instead of 3.0 to 5.0 \AA , while θ has an approximate value of 144° ranging between 120° to 180° [9].

Glass Formers And Modifiers

Several compounds exist in the amorphous phase singly, and all constitute simple glass formers like SiO_2 , GeO_2 , and B_2O_3 [8, 12]. More complex glasses can be produced by introducing other ions into the random network. There are two ways that an ion can enter into a glass; the first is as a network modifier cation or substitutionally for a network former cation. The best mechanism for rare-earth ions turns out to be substitutional. They are conditional glass formers which require more than one additional compound to form glass [12].

Typically in silicate glasses excess oxygen tends to acquire a negative charge. There excess anions that ordinarily bridge two network former cations, instead disrupt the network and become 'non-bridging'. Cations are usually the network modifiers that occupy random areas in the network (see figure 2c) near these non-bridging oxygen to achieve charge-neutrality. This last description of network modifiers best

describes the sort of glasses studied here. Figure 4 illustrates a schematic representation of both bridging and non-bridging oxygen [12] .

As mentioned above, amorphous solids are not like crystals, because each ion has its own unique environment. Furthermore, amorphous solids are often mixtures of many other components producing differences in nearest-neighbor bonding ions. Many different types of ions tend to increase the statistical distribution of neighboring ions eliminating any reoccurring patterns. Neighboring ions find themselves at statistically unequal distances since there are no recurring patterns. Hence, local fields of individual ion sites vary. The consequences are site-to-site differences in the energy levels, radiative and non-radiative transition probabilities, and local coordination structures of optically active ions in glass hosts [13] . A superposition of individual ions that are scattered throughout the ensemble of local environments that contributes to broadband excited optical absorption, emission spectra, and excited state decays. This statistical broadening is known as the inhomogeneous linewidth. The spectrum of amorphous solids demonstrate inhomogeneous broadening, and the decay rates do not demonstrate a single exponential time dependence [5] .

Phonon-Assisted Energy Transfer

In glasses the homogeneous linewidths of optical transition in the rare earths are typically much smaller ($\sim 1 - 10\%$ or less) than the inhomogeneous widths. As

noted above, the inhomogeneous width results from the statistical distribution of Stark-shifted excited states that are a consequence of the large number of different environments that are possible in a disordered matrix.

When a transition is excited by a light source whose linewidth is small compared to the homogeneous width, and observed under time resolution, the prompt fluorescence has a width equal to twice the homogeneous width of the transition. (The factor of two occurs because both the excitation and the emission are broadened.) If the radiative lifetime of the transition is sufficiently long, it is commonly observed that the width of the transition broadens with time, becoming several times the homogeneous width before the fluorescence becomes too weak to be observed. This time-dependent broadening, which is commonly called spectral diffusion, energy migration, excitation transfer, or energy transfer, is possible only if ions with energies outside the set of sites which received the original excitation are promoted to the excited state and subsequently fluoresce. Energy conservation requires that for the excitation to migrate to a state of higher (lower) energy, some other excitation of the sample must be destroyed (created) to make up the energy difference. Phonons provide such a set of excitations that can conserve energy. Phonons couple to the electronic states through their modulation of the local electric fields produced by neighboring atoms in the glass. Figure 5 diagrams a one-phonon-assisted energy transfer process. Energy transfer involving multiple phonons is also possible. The

theoretical treatment of Holstein, Lyo, and Orbach [14] for a Debye phonon spectrum shows that the lines should broaden uniformly from energy transfer.

Results of Powell and Gang

Probing the singlet-singlet ${}^5D_0 - {}^7F_0$ fluorescence in Eu^{3+} -doped glasses with time-resolved site-selection spectroscopy following laser excitation between these two states, Powell and Gang [3] reported growth of discrete structures in the wings of the fluorescence. They observed that the smooth shoulders of the fluorescence spectrum evolved distinct side peaks displaced a few cm^{-1} from the excitation frequency. They attributed these phonon-assisted energy transfer to preferred sites within the glass, i.e., to those that produce the same Stark shift for large numbers of Eu^{3+} ions. Since there are no corresponding structures in the absorption spectrum of the glass, these preferred sites must represent correlation with those at the energy of excitation rather than sites preferred absolutely. Such structures had not been seen previously as they are easily obscured in transitions involving states with multiple Stark components. Stark components arise when a multiplet level is split by an electric field.

Noting that the side peaks seen by Powell and Gang [3] are spaced at nearly equal frequency intervals, Dixon [15] proposed an alternative explanation. He suggested that as one reaches the mobility edge (the frequency at which phonons are localized by the disorder in the glass), the amplitudes of the phonons abruptly grow in

order to accommodate a quantum of vibrational energy on a much smaller number of atoms. These large amplitude coherent motions are more strongly coupled to the electronic states, and the structures seen by Powell and Gang [3] represent multiples of the mobility edge.

The purpose of the present study is to extend the energy transfer investigation to additional Eu^{3+} -doped glasses and to attempt to distinguish between these two proposals.

Statement of Purpose

This study here reports on the ${}^5\text{D}_0 - {}^7\text{F}_0$ transition of Eu^{3+} ions using resonant excitation with fluorescence line narrowing (FLN). The purpose of this experiment is to study energy transfer in glasses doped with Eu^{3+} ions and column one elements. This study avoids one of the major problem of multiple Stark components met with by others, Motegi and Shionoya [5]. Stark components arise when a multiplet energy level is split by an electric field. A Nd:YAG laser was used for site-selection spectroscopy, using FLN. FLN allows the studying of local dynamic effects that were once masked by inhomogeneous broadening. Pulse duration was 5.0 ns allowing time dependent studies on the scale of milliseconds. The level of discrete structure, lifetimes, linewidths, energy transfer rates, and temperature-dependent parameters all change for the various types of glass hosts [3]. The source of all variables between

glasses of the same chemical composition can be attributed to differences in local order [2] . This system allows for studying of energetically distinct subsets of Eu^{3+} ions in four glasses. The data acquired during this experiment will be shown to compared to a model developed by Dixon.

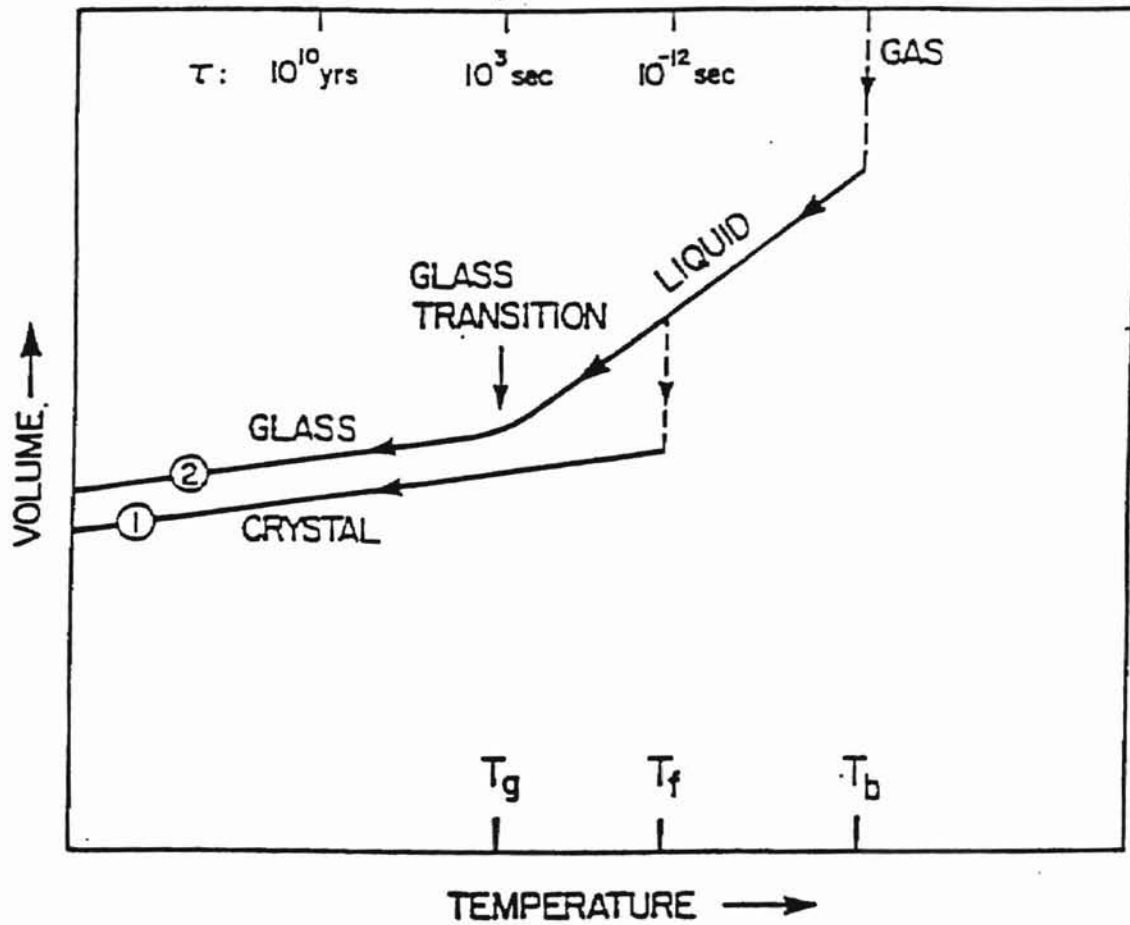


Figure 1: The two general cooling paths by which an assembly of atoms can condense into the solid state. Scenario 1 is the path to the crystalline state; scenario 2 is the rapid-quench path to the amorphous solid state.

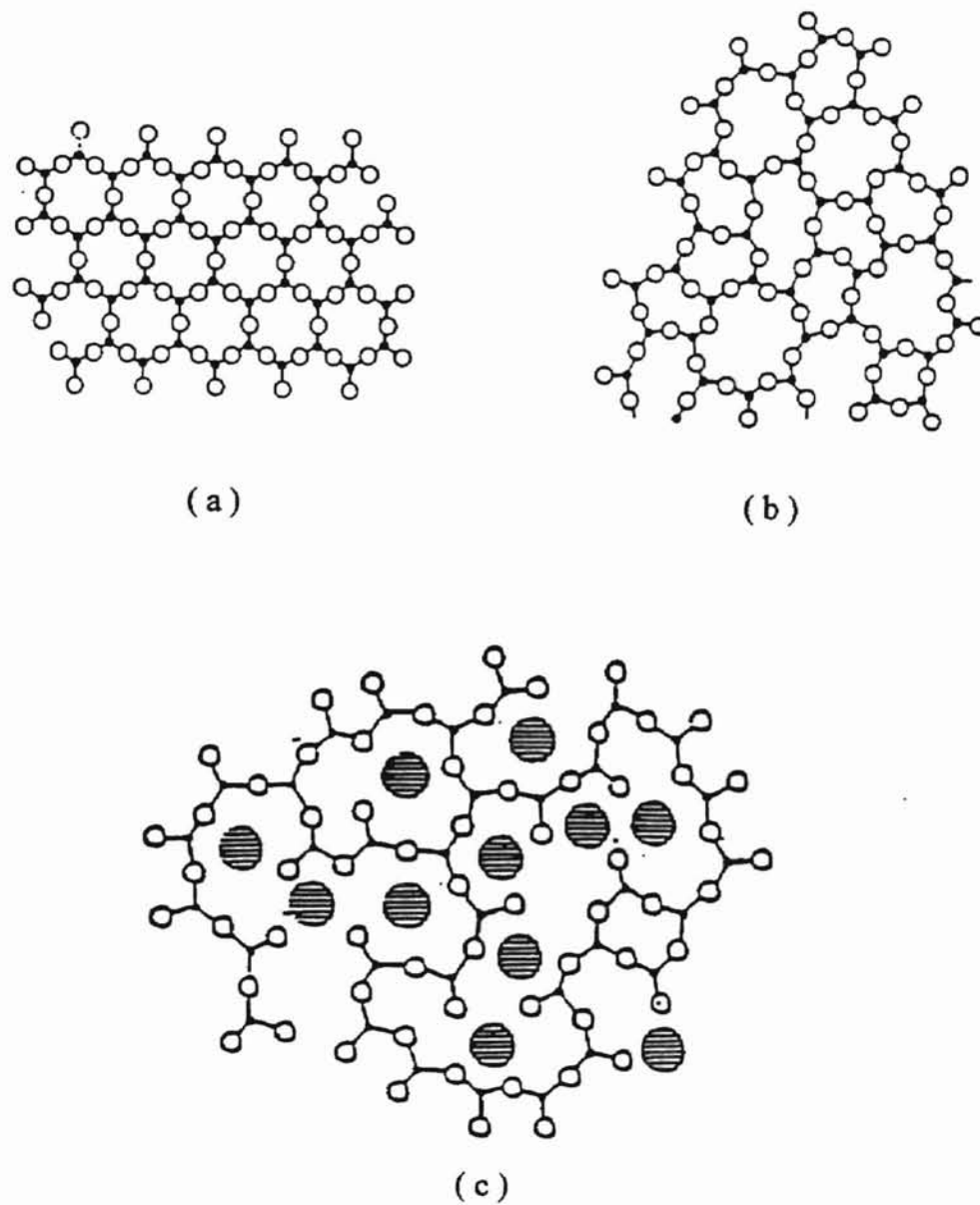


Figure 2: Two dimensional schematic of the structure of (a) crystalline SiO_2 , (b) is a SiO_2 glass, and (c) $\text{M}_2\text{O-SiO}_2$ glass. The small solid circles are the silicon atoms, open circles the oxygen atoms, and the large shaded circles the alkali atoms.

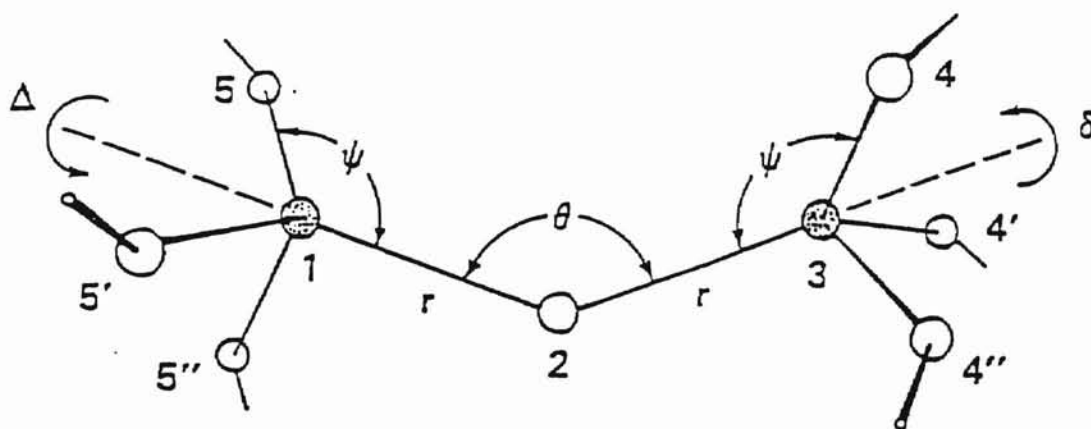
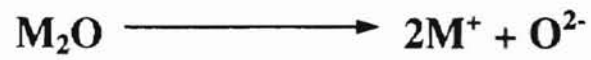


Figure 3: The relative orientation of two corner sharing tetrahedra in SiO_2 , showing the short range order and one aspect of the intermediate range order. The Si atoms (dark) are surrounded tetrahedrally at distance r by four O atoms and each O atom bridges between two Si atoms with an angle θ that varies from site to site. This specifies the SRO. The dihedral angles δ , Δ , giving the angular orientation of tetrahedra about their bridging O-Si bonds, are defined in this paper as elements of IRO.



BRIDGING

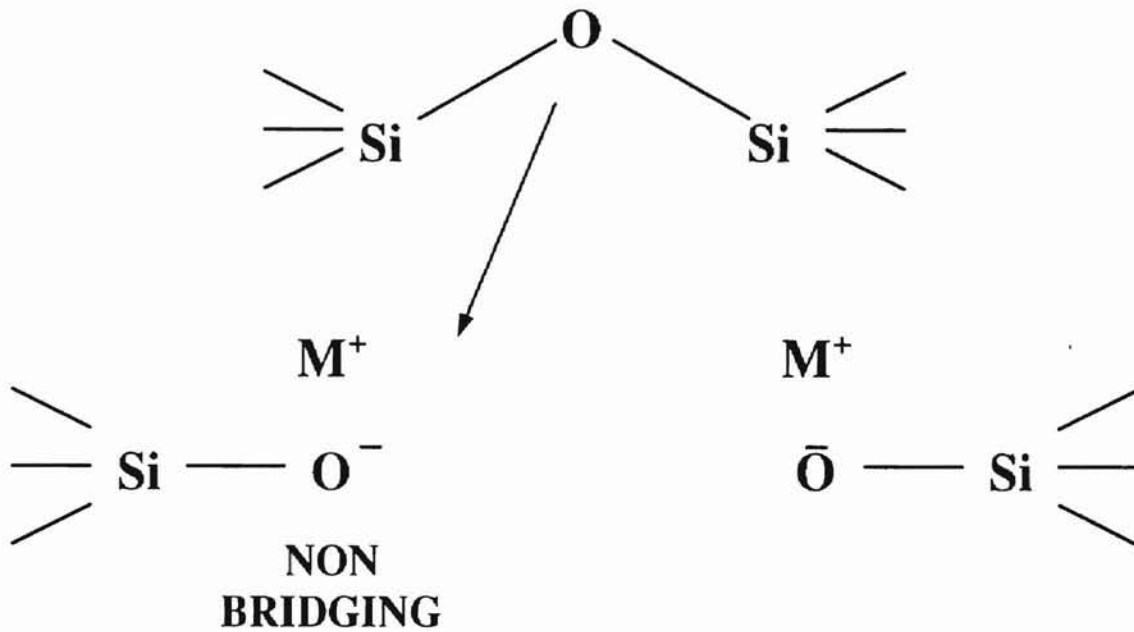


Figure 4: Schematic representation of the formation of non-bridging oxygen in silicates on dissolution of alkali oxide.

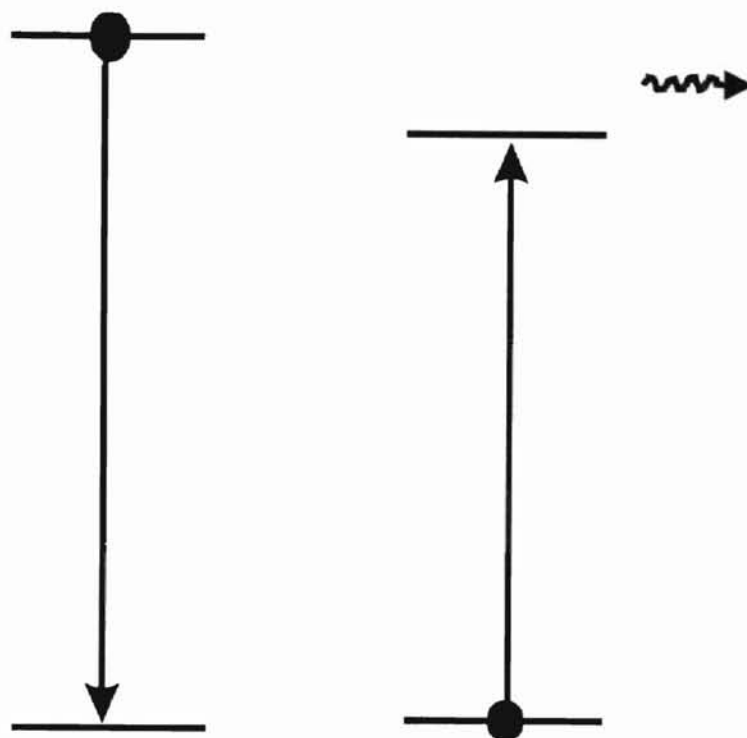


Figure 5: Schematic representation of a single-phonon-assisted energy transfer process.

CHAPTER II

EXPERIMENTAL

Samples

The four sample glasses studied in this investigation all have similar chemical formulas, as seen in Table I. The LS glass, which was also studied by Powell and Gang [3], was used as a control sample. Each sample in this investigation contained 5.0 percent Eu^{3+} ions except the control sample which contain only 3.0 percent. Also, each sample contained a different alkali element. These alkali elements are network modifiers.

These glasses were given to us by Powell [3] . Sample sizes ranged from 3.0 x 3.0 x 10.0 mm to 3.0 x 3.0 x 20.0 mm. Each sample went through a series of steps before they were mounted in the cold finger. Step one, consisted of polishing each sample to optical quality. Step two, absorption spectra were taken for each glass. That were performed using a Cary 05 spectrophotometer at room temperature with a 50 W Xenon lamp.

TABLE I

SAMPLE COMPOSITIONS (mole %)

<u>Sample</u>	<u>Network formers</u>	<u>Network modifiers</u>
* LS	57.0 SiO ₂	27.5 Li ₂ O 10.0 CaO 2.5 Al ₂ O ₃ 3.0 Eu ₂ O ₃
LiSiO	70.0 SiO ₂	15.0 LiSiO 5.0 BaO 5.0 ZnO 5.0 Eu ₂ O ₃
Na	70.0 SiO ₂	15.0 Na ₂ O 5.0 BaO 5.0 ZnO 5.0 Eu ₂ O ₃
Rb	70.0 SiO ₂	15.0 Rb ₂ O 5.0 BaO 5.0 ZnO 5.0 Eu ₂ O ₃

* Indicate that this sample is the control sample.

Experimental Apparatus

The samples in this investigation were mounted in a CTI closed cryogenic refrigerator system. Each sample was placed in the cold finger with a small prism positioned at the bottom of the sample. The prism was used to direct the laser beam up through the sample producing an excited volume (see figure 6). This excited volume effectively fills the 20 x 2.0 mm slit of the SPEX 1404 0.85 m Double Slit Spectrophotometer with scattered light from the sample. The cold finger was then positioned on its side along the optical bench (appropriately 1.0 meter away from the slit) of the spectrophotometer in such away that the laser beam was at an angle of 90 degrees to the 1404 spectrophotometer's slit. This was done in order to keep direct laser light from damaging the phototube.

The experimental setup can be seen in figure 7. A Continuum Nd:YAG Pulse Laser was used to pump a DL II Series Dye Chamber, which allowed tuning flexibility. The use of an attenuator between the laser and the Dye Cell Chamber enabled variance in the output power of the laser, operating at 532 nm. This was very important because anything over 100 mW would burn the curvets, which contained Rhodamine 6G dye. The Rhodamine 6G dye was utilized in the oscillating and amplifier curvets in concentrations of 144 mg/100 ml and 72 mg/100 ml respectively. So, the attenuator was set to give an approximately reading of 80.0 mW. This power

reading was constantly monitored throughout the entire experiment once at the beginning and several times during the experiment with a power meter.

Two specially coated mirrors, for the second harmonic, were utilized to direct the beam into the attenuator. They also pass the 1064 nm fundamental to a beam dump. The beam was then aligned through the DL II Dye Cell Chamber. Two additional mirrors were used after the Dye Cell Chamber to direct the beam up and across to the other table. The beam was then refocused using a 10.0 cm lens this sharpen the image of the beam through the windows of the cryostat. Therefore, the beam could be tightly focused on the prism. This was accomplished by mounting the 10.0 cm lens on a series of bases so that its horizontal and transitional motion could be adjusted anywhere from a few centimeters to a few millimeters. After the beam had been focused onto the prism and all the fine adjustments have been made to maximize the fluorescence of the beam and the sample. A 50.0 mm lens was used to collect and collimate the fluorescence which was then collected by a 62.9 mm lens. The 62.9 mm lens focused the fluorescence to a sharp line that was at the center of an electronic shutter. The electronic shutter was used to block out the scattered light from the laser, because it could damage the RA 43-02/1000/1001 photomultiplier tube. Then it was collected once again and focused in such away to totally fill the 20.0 by 5.0 mm slit of the spectrophotometer.

Once the fluorescence has been tightly focused into the slits of the spectrophotometer, the width of the slits can be adjusted to control the actual amount

of light that goes to the photomultiplier tube. The first slit was set to 100 μm while the two slits in the middle were wide open and the last slit before the photomultiplier tube was also set to 100 μm . The photomultiplier tube was powered by a SPEX modified 286 computer. The SPEX 286 computer was equipped with several input boards that allowed control of the voltage of the PMT, the spectrophotometer, and the data acquisition system module from the integrator unit. The signal which was seen first on the oscilloscope registering in the millivolt range and then on to a Boxcar Averager/Integrator unit which was in tandem with a Signal Processor. These units averaged the incoming voltages smoothing out some of the background noise at an estimated signal to noise ratio of 10.0. This improved signal was then sent to the computer via the DM303M module and was plotted on the computer screen as an inverse graph. The internal controls of the SPEX program allowed me several other ways of averaging the data. One way was by averaging multiply scans, and another way was by averaging over several points per step. This allowed improvement of the signal to noise ratio by another factor of 3.0.

Experimental Procedures

After the sample has been securely mounted in the cold finger of the CTI closed cryogenic refrigerator system, the system was rough pumped to 100/50 mTorr. At which point the diffusion pump took the system down to approximately 5 to 10

mTorr. The system was allowed to pump down overnight to insure a good vacuum before turning on the compressor. The following day the compressor was turned on, and the set point on the temperature controller was set for 70 K. While waiting on the cryostat temperature to reach the set point the laser was turned on to ensure thermal stabilization of the power of the laser.

This experiment employs the method of time resolved, site-selection spectroscopy utilizing the technique of fluorescence line-narrowing (FLN). A standard monochromatic source could be used in FLN experiments, but the spectroscopic tool of choice is a tunable laser. The laser used in this experiment was a Nd:YAG laser, with pulse duration of approximately 5.0 ns with a bandwidth between 2.0 to 3.0 nm. The Nd:YAG laser was used to excite an energetically selected subset of Eu^{3+} ions within an inhomogeneously broadened absorption profile. This technique is called fluorescence line narrowing spectroscopy. The Model TI32 Shutter Driver/Timer was used as a way to minimize the amount of scattered light that might enter into the 1404 spectrophotometer. The shutter was set to open 13.4 ms before the laser pulse passed through the shutter with an exposure time of 34.2 ms. The emission from this subset was measured by gated detection utilizing a Model 4420 Gated Integrator & Model 4402 Boxcar Averager system. The measurements were relayed to the detection system via a RA 43-02/1000/1001 photomultiplier tube set at 1500 volts. The gated detection allowed measurement of the emission before substantial cross

relaxation could occur between ions in different sites, allowing an emission spectrum of only those ions initially excited [3, 16] .

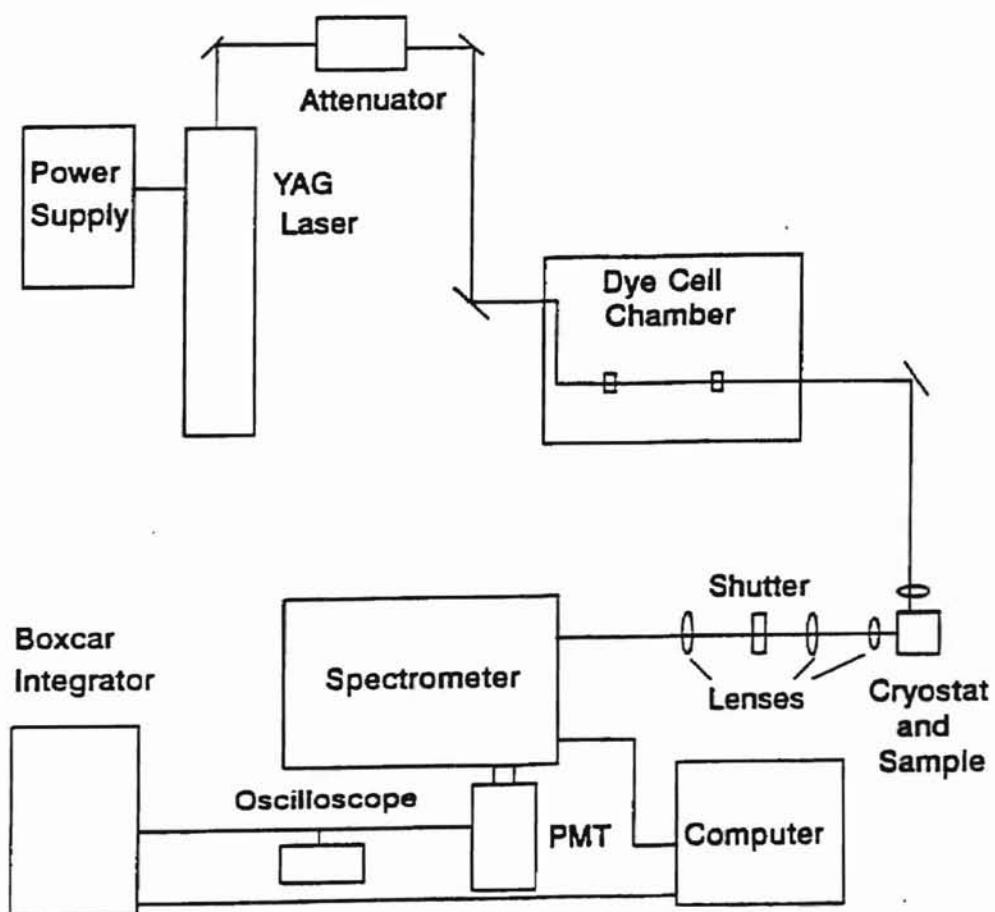


Figure 6: Site-selection spectroscopy using fluorescence line-narrowing experimental equipment diagram for the study of energy transfer in glasses doped with Eu^{3+} ions.

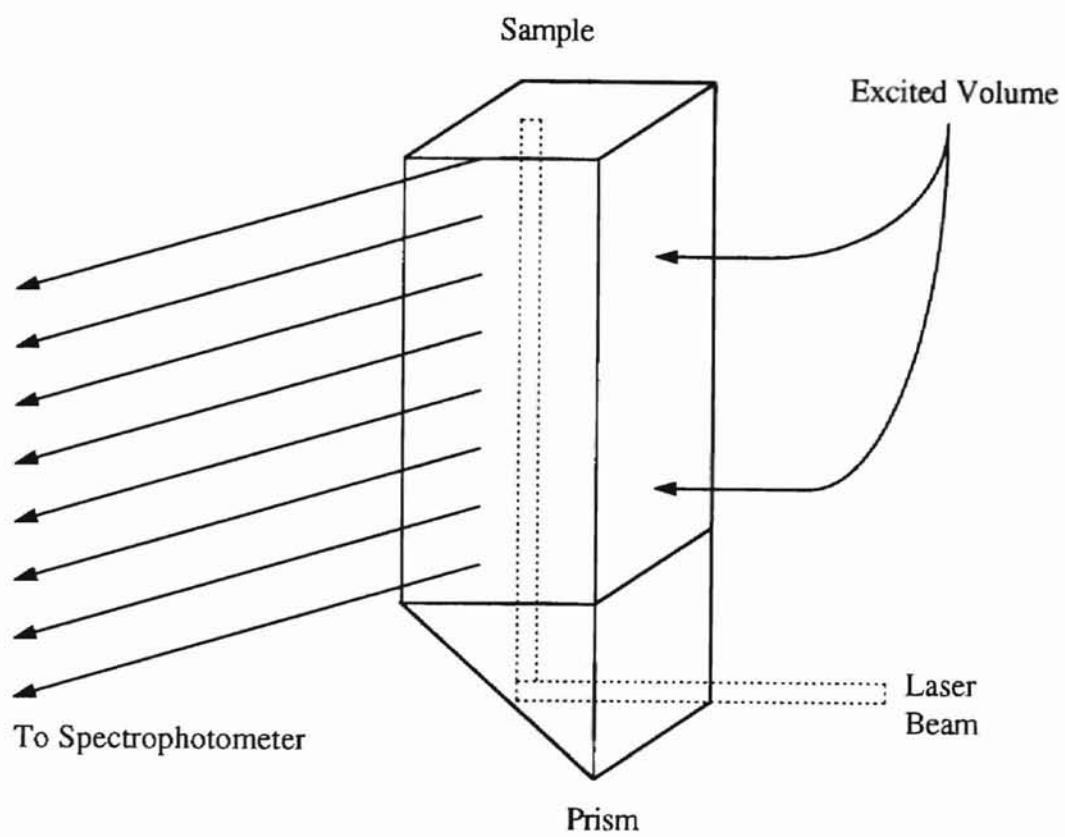


Figure 7: Experimental sample arrangement and orientation to the spectrophotometer

CHAPTER III

RESULTS AND DISCUSSION

Current Model

The model used here hypothesizes that the disordered structure of the glasses leads to weakly localized phonons [15]. This model attempts to explain the thermal transport properties of glasses at temperatures well above the plateau that occurs in thermal conductivity experiments [17] as well as energy transfer. Thermal conductivity experiments suggest that these weakly localized phonons are mediators of heat energy. Golding et al. [18] have argued the point that this plateau represents a region where thermal phonons correlation lengths, ξ , to be less than their wavelength. The intrinsic disorder of glassy material lends itself to the consequences of weak localization.

Holstein, Lyo, and Orbach [14] introduced a general method to describe energy transfer among optically active ions mediated by Debye phonons. A modification proposed by Dr. Dixon [15] takes into account some of the features of the phonon localization that is caused by the disorder in the glass network. In this model the localized phonons near the mobility edge produce an enhanced energy transfer rate.

This enhancement is due to the larger amplitude that a localized phonon must have in order to accommodate quantum of energy $h\nu$ on a small ($\sim 10^{10}$) number of atoms rather than all 10^{21} or so in the entire sample. This large amplitude modulates the electric field of the surrounding ions and thus strongly couples the localized phonons to the electronic states of the optically active ions. This enhanced energy transfer can be seen using time resolved site-selection spectroscopy as a series of side peaks in the fluorescence spectrum. These side peaks in the fluorescence spectrum were also reported by Powell and Gang [3] as discussed above.

The energy transfer mediator probabilities as presented by HLO [14] for one or two phonons, take the form:

$$W_{2\leftarrow 1}^- = \frac{2\pi}{\hbar} J^2 (f-g)^2 \sum_{\alpha} \frac{|\langle n_{\alpha} - 1 | \Delta \epsilon | n_{\alpha} \rangle|^2}{(\Delta E_{12})^2} \delta(\Delta E_{12} - \hbar\omega_{\alpha}), \quad (4)$$

$$W_{2\leftarrow 1}^- = \frac{2\pi}{\hbar} J^2 (f-g)^4 \sum_{\alpha\beta} \frac{|\langle n_{\alpha} - 1 | \Delta \epsilon | n_{\alpha} \rangle|^2}{(\hbar\omega_{\alpha})^2} \frac{|\langle n_{\beta} - 1 | \Delta \epsilon | n_{\beta} \rangle|^2}{(\hbar\omega_{\beta})^2} \delta(\Delta E_{12} - \hbar\omega_{\alpha} - \hbar\omega_{\beta}), \quad (5)$$

$$W_{2\leftarrow 1}^- = \frac{2\pi}{\hbar} J^2 (f-g)^4 \sum_{\alpha\beta} \frac{|\langle n_{\alpha} - 1 | \Delta \epsilon | n_{\alpha} \rangle|^2}{(\hbar\omega_{\alpha})^2} \frac{|\langle n_{\beta} + 1 | \Delta \epsilon | n_{\beta} \rangle|^2}{(\hbar\omega_{\beta})^2} \delta(\Delta E_{12} - \hbar\omega_{\alpha} + \hbar\omega_{\beta}), \quad (6)$$

with J as the inter-ionic coupling, f and g are the electron-phonon coupling to the excited state, and ground state, respectively. Here ΔE_{12} represents the difference in (excited state energies) the two ions excited state energies, and $\Delta \epsilon$ is the local strain at

donor and acceptor ions due to interacting phonons. These two equations are only for phonons being emitted and not for absorption. Their corresponding absorption equations are respectively $W_{2\leftarrow 1}^+$ and $W_{2\leftarrow 1}^{++}$. Higher order electron-phonon coupling constants have been left out to simplify this model [12, 13].

Raman spectra of these glasses indicate both low frequency extended phonons and localized phonons above a minimum frequency, the mobility edge [15, 17] (see figures 8 -11). The mobility edge presented here is representative of the onset of Raman activity at low frequencies, that implies an onset of phonon localization. Raman activity for this family of glasses begins between 5 - 20 cm^{-1} . The boson peaks for this family of glasses range from 20 - 80 cm^{-1} (see Table II). The boson peak for this family of glasses tends to shift to low frequencies as the size of the network modifier ions increases.

The LS-modified members of this family are worth a closer examination, because calculations from the model does a fairly decent job modeling the experimental data. The fluorescence spectrum was assumed to be proportional to the rate of single-step energy transfer to states outside the excitation band. This rate is dependent on several factors: linewidth of the laser, donor and acceptor ions along with the spectral density of acceptor ions. The transfer probabilities were calculated on infinitesimally sharp states. These results have been combined with the a Lorentzian width of 4.0 cm^{-1} . Finally, acceptor ions spectral density was estimated

TABLE II

RISING EDGE OF THE BOSON PEAKS

Samples	Boson Peak Edge Wavenumbers	Boson Peak Edge Frequency(10^{11})
LS Glass	14.0 cm^{-1}	4.2 Hz
LiSiO Glass	13.0 cm^{-1}	3.9 Hz
Na Glass	10.0 cm^{-1}	3.0 Hz
Rb Glass	5.0 cm^{-1}	1.5 Hz

from the inhomogeneously broadened absorption band. The mobility edge was adjusted to 17 cm^{-1} to locate the one-phonon absorption peak for an excitation of 17238 cm^{-1} . A sound velocity of $3.0 \times 10^5 \text{ cm/s}$ with a correlation length of 17 cm^{-1} Debye phonon. While the electron-phonon coupling terms ($f - g$) were chosen to be 950 cm^{-1} to estimate the relative peak height of the 17238 cm^{-1} . Last, the amplitude of the fluorescence was adjusted with respect to Powell and Gang's [3] data. The agreement between calculation and experiment is very supportive of the model.

Spectral Structures

Figures 12 - 15 shows absorption spectra while figures 16 - 27 shows laser-excitation spectra for LS, LiSiO, Na, and Rb glasses under three different excitation conditions. The emission spectra here have been normalized with respect to their absorption spectra. The excitation spectrum were recorded with a $298 \mu\text{s}$ gate width and a 13.4 ms delay after the excitation pulse along with a 32.0 ms exposure constant. Spectra were obtained from the low- and high-energy sides of the absorption band. The spectra were obtained at a temperature (70 K) where spectra structure was expected to be its strongest. The respective spectra evolve over time due to ion-ion energy transfer between different sites. After the excitation pulse, spectral structures start to develop at times greater than 1.0 ms . This can be

observed in the figures 16 - 27. A discussion of the spectral structures seen in the graphs will be discussed and possible reasons behind these spectral structures.

Figures 16 - 27 presents the growth of discrete structured regions (side peaks) across the spectral band as time elapses after the initial excitation pulse. Some structures are more distinctive in different glasses containing different modifiers and different former elements. Powell and Gang [3] noticed similar structured regions (side peaks) across their samples' spectrums. Their proposed answers to these structured regions (side peaks) were mentioned above, but are worth mentioning again briefly. They proposed that these structured regions (side peaks) are due either to a maximum amount of disorder or a higher degree of local order in the host glasses [3]. Since glass itself is a disordered system to start with anything added to the system must either aid in building or destroying the network. The column one elements, network modifiers, pulls the network apart as seen in the Zachariasen model [8] (see figure 2) leaving bridging and non-bridging oxygens. The heavier modifier ions was proposed to produce a higher degree of local order leading to an increase in ion-ion energy transfer, which implies more side peaks. This was the hypothesis by Powell and Gang [3] in 1984. Alternately, there maybe a correlation between side peaks and the phonon mobility edge.

The model proposed by Dixon [15] relates peak spacing to the low frequency mobility edge for phonon localization. The key feature of energy transfer that produces side peaks due to enhanced transfer at the mobility edge is

that the side peaks should have equal separations in energy. Figure 28 demonstrates that a correlation exists only for the Li glasses where the peaks are spaced at multiples of the mobility edge. While all members of this family of glasses are spaced at equal multiples of the common 0.4 THz. (see figure 29 and Table III) This suggests a localized phonon characteristic of a Eu^{3+} containing clusters rather than the overall mobility edge is responsible for the side peaks. It is unlikely that evenly separated structures would result from the mechanism proposed by Powell and Gang [3] .

The full widths at half maximum (FWHM) of the glasses presented here can be seen in figures 30 - 32. These FWHM graphs demonstrate a migration of energy outward over time. This provides evident of energy transfer out of different sites over the specified time intervals. While figures 33 - 35 illustrates how the width of the peak dissipate over time. The LS glass has the fastest dissipation of energy out of the initial site, while the LiSiO glass illustrates the slowest.

TABLE III

ONSET OF RISING EDGE OF LOW FREQUENCY
BOSON PEAKS AND OF SECONDARY PEAKS

Network Modifiers	λ_{ex} (nm)	1 st Minimum (10^{14} Hz)	2 nd Minimum (10^{14} Hz)	3 rd Minimum (10^{14} Hz)	4 th Minimum (10^{14} Hz)
LS	578	5.185	5.181	5.176	5.172
	579	5.175	5.171	5.167	-
	579	5.185	5.188	5.192	-
	580	5.176	5.181	5.185	5.189
LiSiO	578	5.184	5.180	5.176	5.173
	579	5.177	5.174	5.171	-
	579	5.185	5.189	5.193	-
	580	5.176	5.180	5.184	5.189
Na	578	5.185	5.181	5.177	-
	579	5.177	5.173	5.170	-
	579	5.185	5.191	5.193	-
	580	5.176	5.180	5.184	-
Rb	578	5.185	5.181	5.177	-
	579	5.176	5.172	5.167	-
	579	5.185	5.188	5.191	-
	580	5.175	5.179	5.183	-

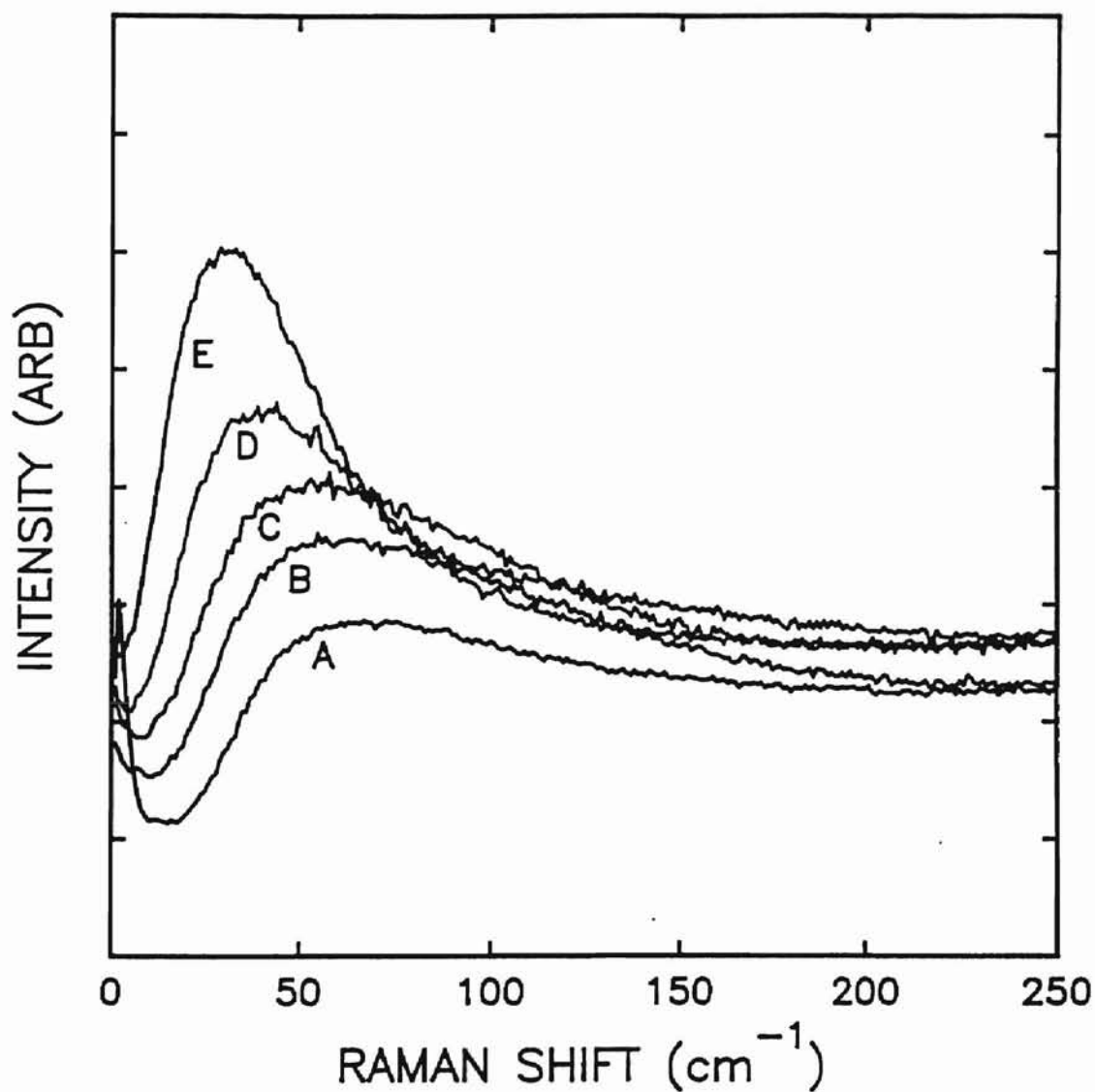


Figure 8: Raman spectra of the glasses. All data were obtained at room temperature. The low frequency region of the boson peak is shown for all three members of this series of glasses. Curve A is the LiSiO glass; curve B is the Na-modified glass; curve D is the Rb-modified glass, while curve C and E are not used in this study.

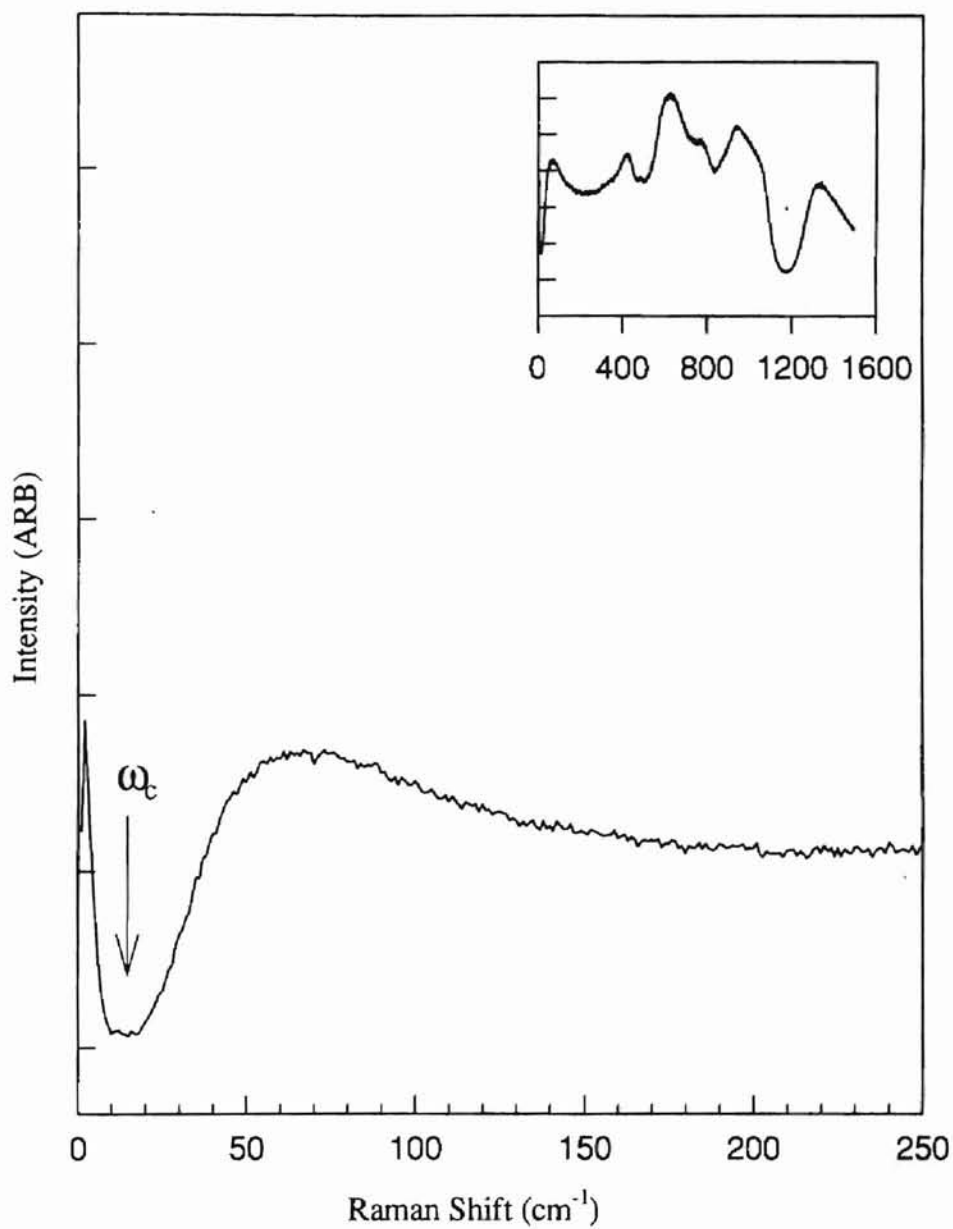


Figure 9: Raman spectra of LiSiO glass. All data were obtained at room temperature. The low frequency region of the boson peak is shown for the LiSiO glass in this series of glasses. The inset is a full Raman spectrum of the LiSiO modified glass.

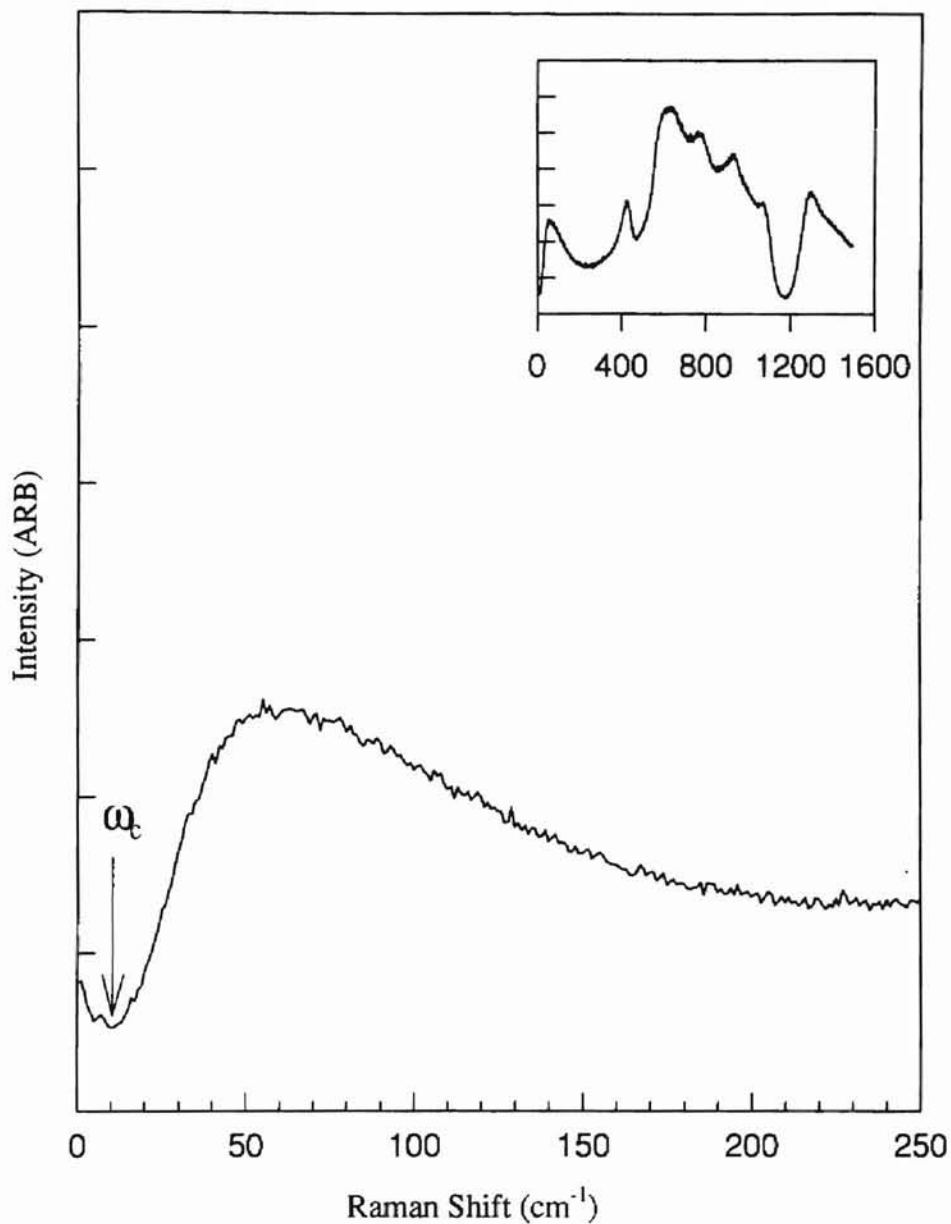


Figure 10: Raman spectra of Na glass. All data were obtained at room temperature. The low frequency region of the boson peak is shown for the Na glass in this series of glasses. The inset is a full Raman spectrum of the Na modified glass.

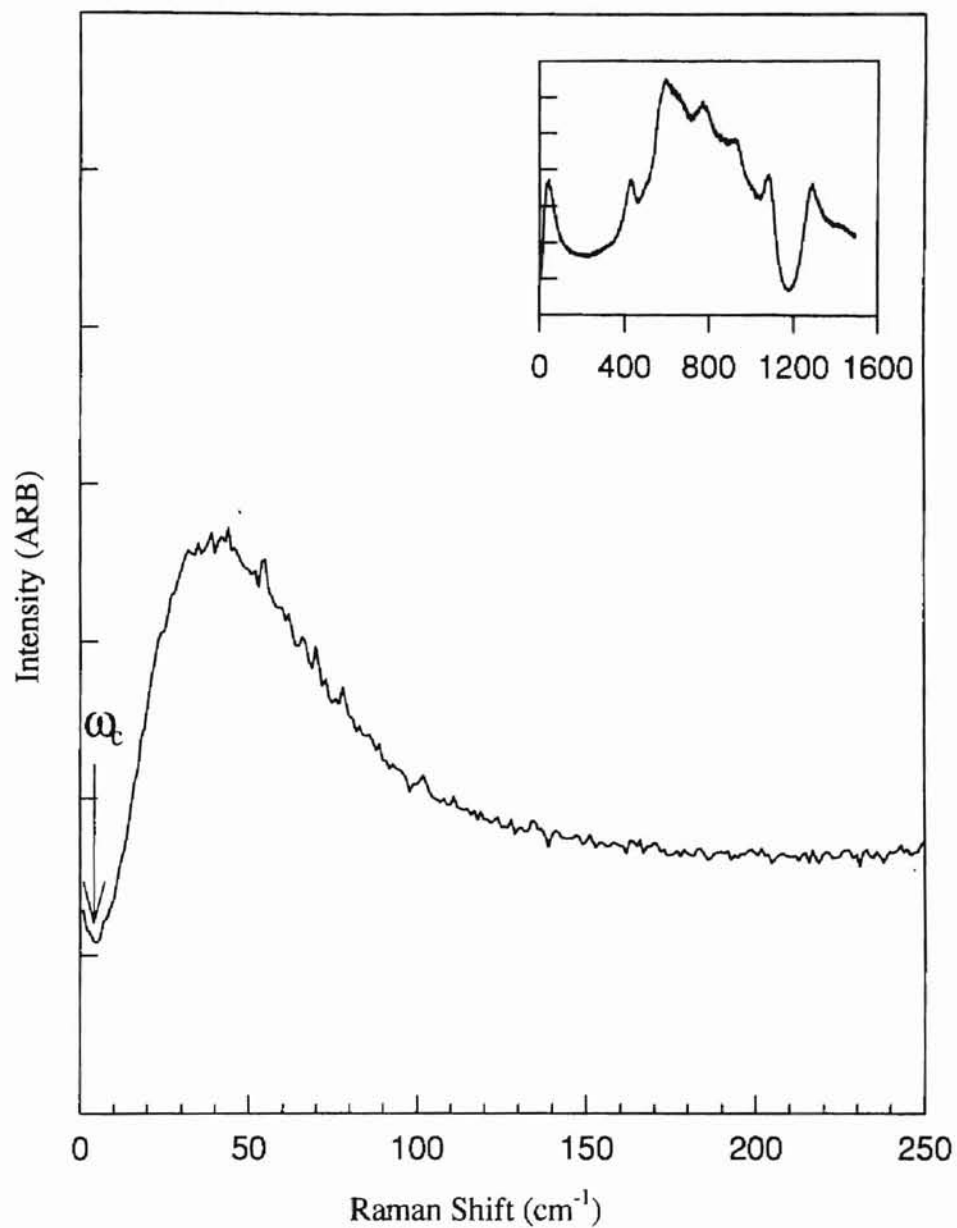


Figure 11: Raman spectra of Rb glass. All data were obtained at room temperature. The low frequency region of the boson peak is shown for the Rb glass in this series of glasses. The inset is a full Raman spectrum of the Rb modified glass.

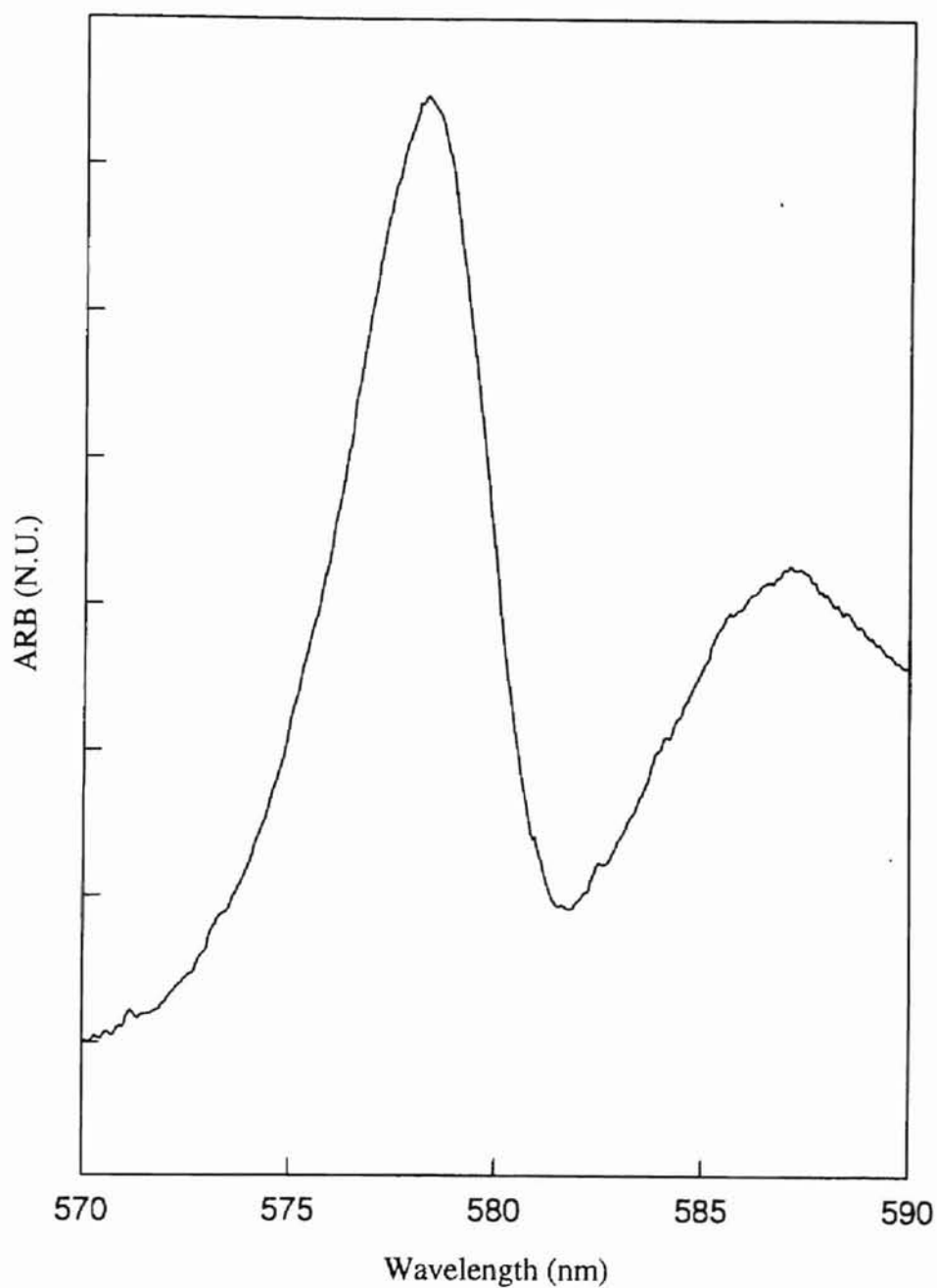


Figure 12: The absorption spectra for LS glass over a spectrum range of 570 - 590 nm performed at room temperature on a Cary 05 spectrophotometer.

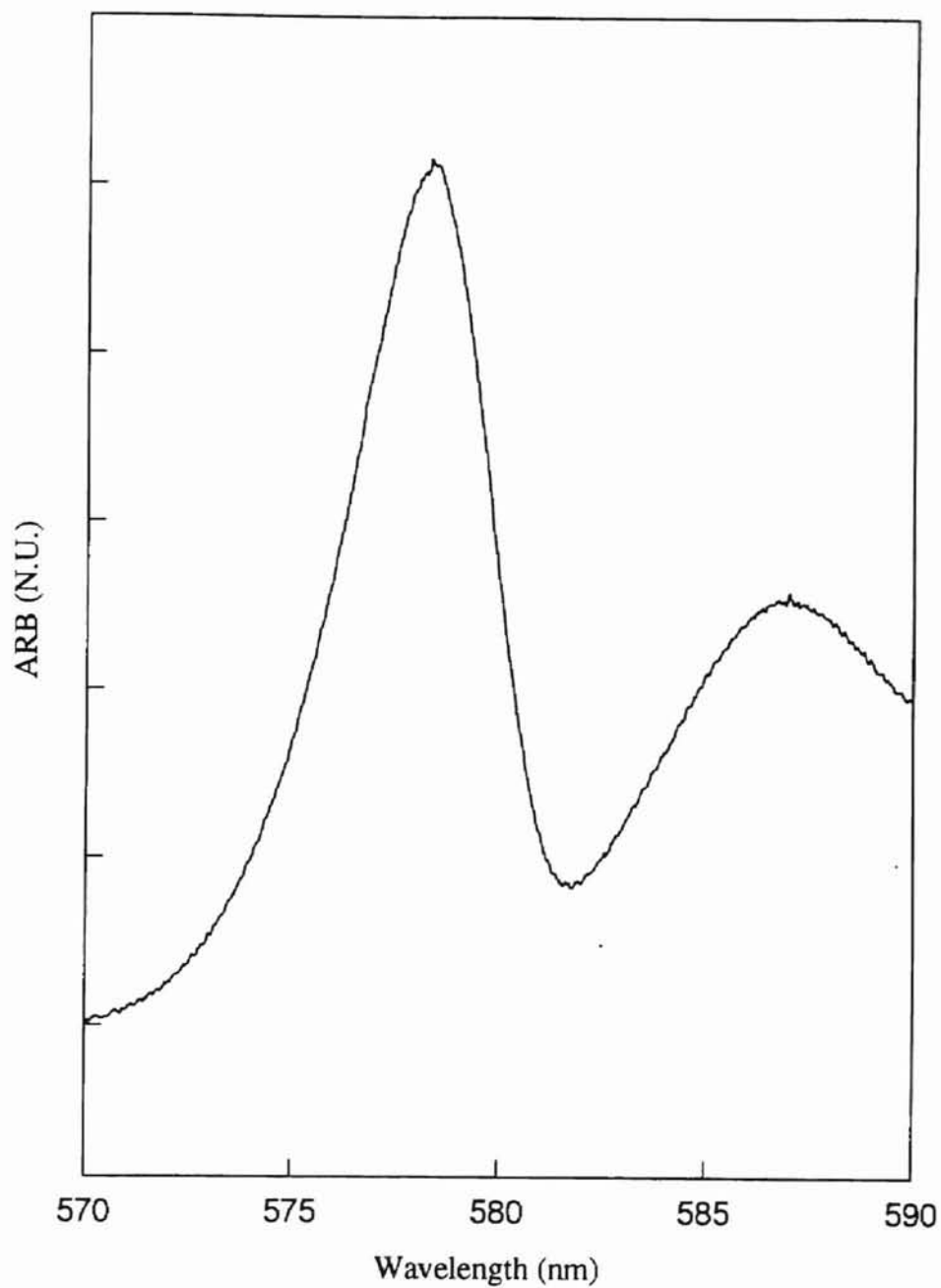


Figure 13: The absorption spectra for LiSiO glass over a spectrum range of 570 - 590 nm performed at room temperature on a Cary 05 spectrophotometer.

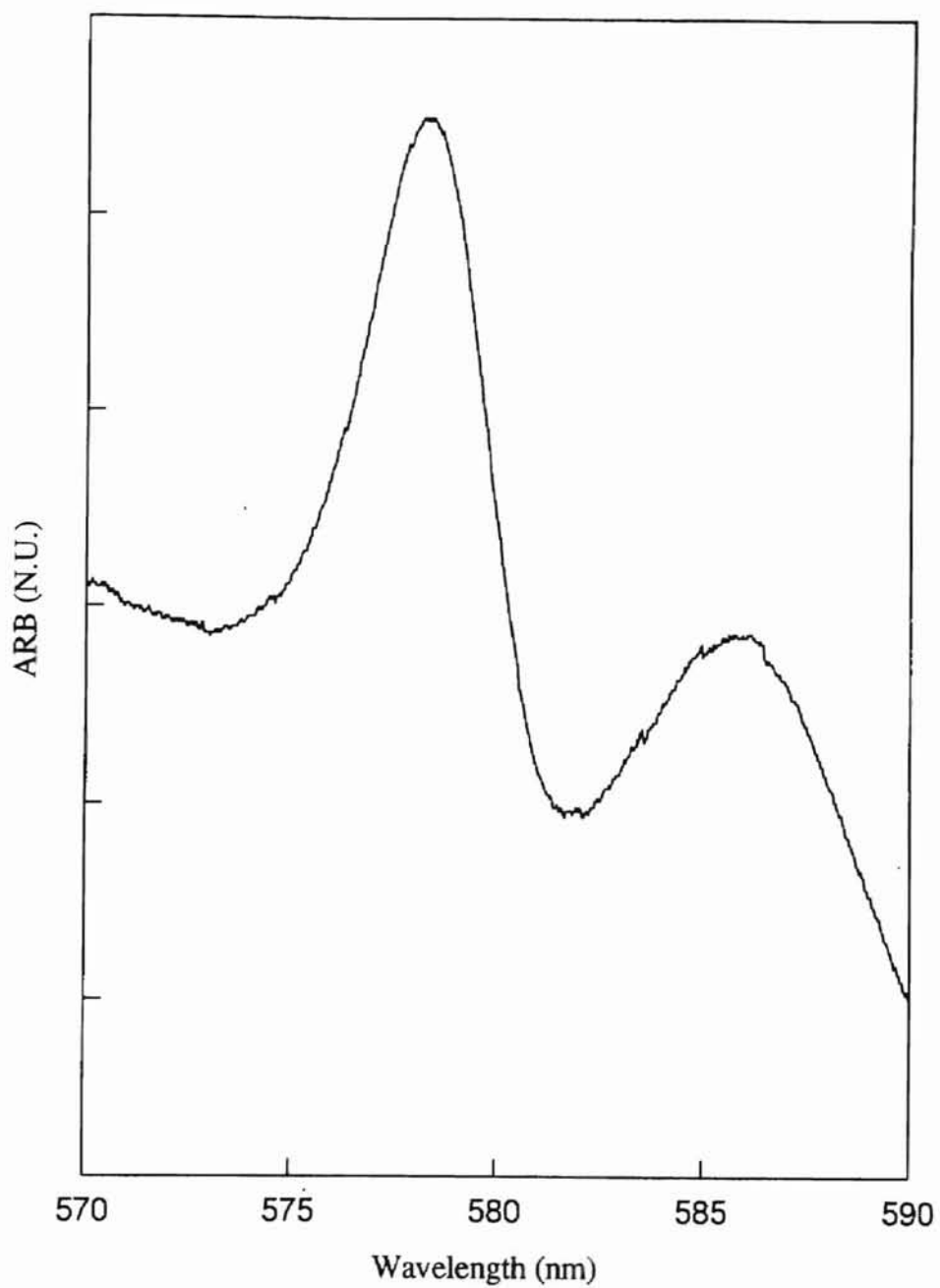


Figure 14: The absorption spectra for Na glass over a spectrum range of 570 - 590 nm performed at room temperature on a Cary 05 spectrophotometer.

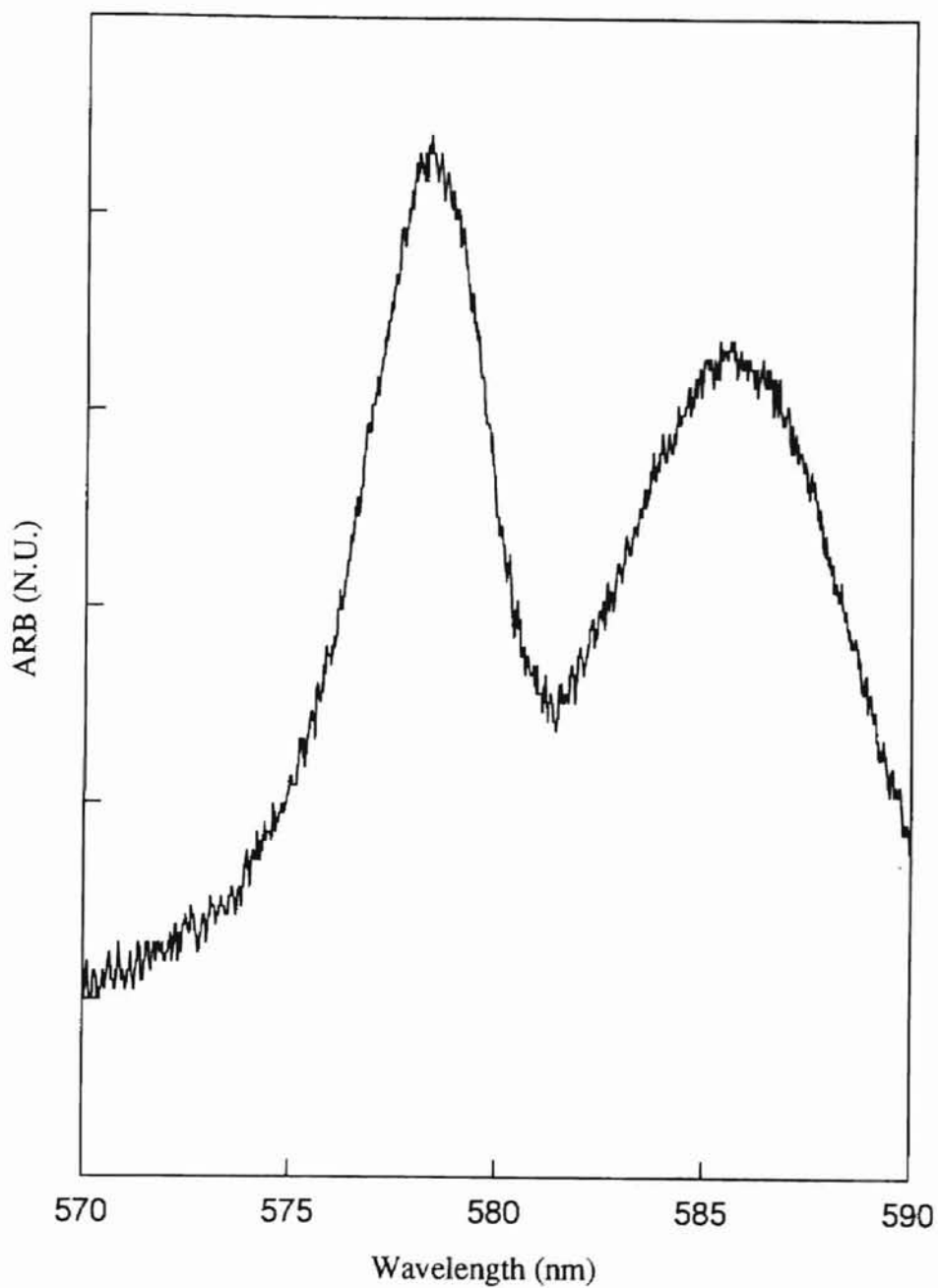


Figure 15: The absorption spectra for Rb glass over a spectrum range of 570 - 590 nm performed at room temperature on a Cary 05 spectrophotometer.

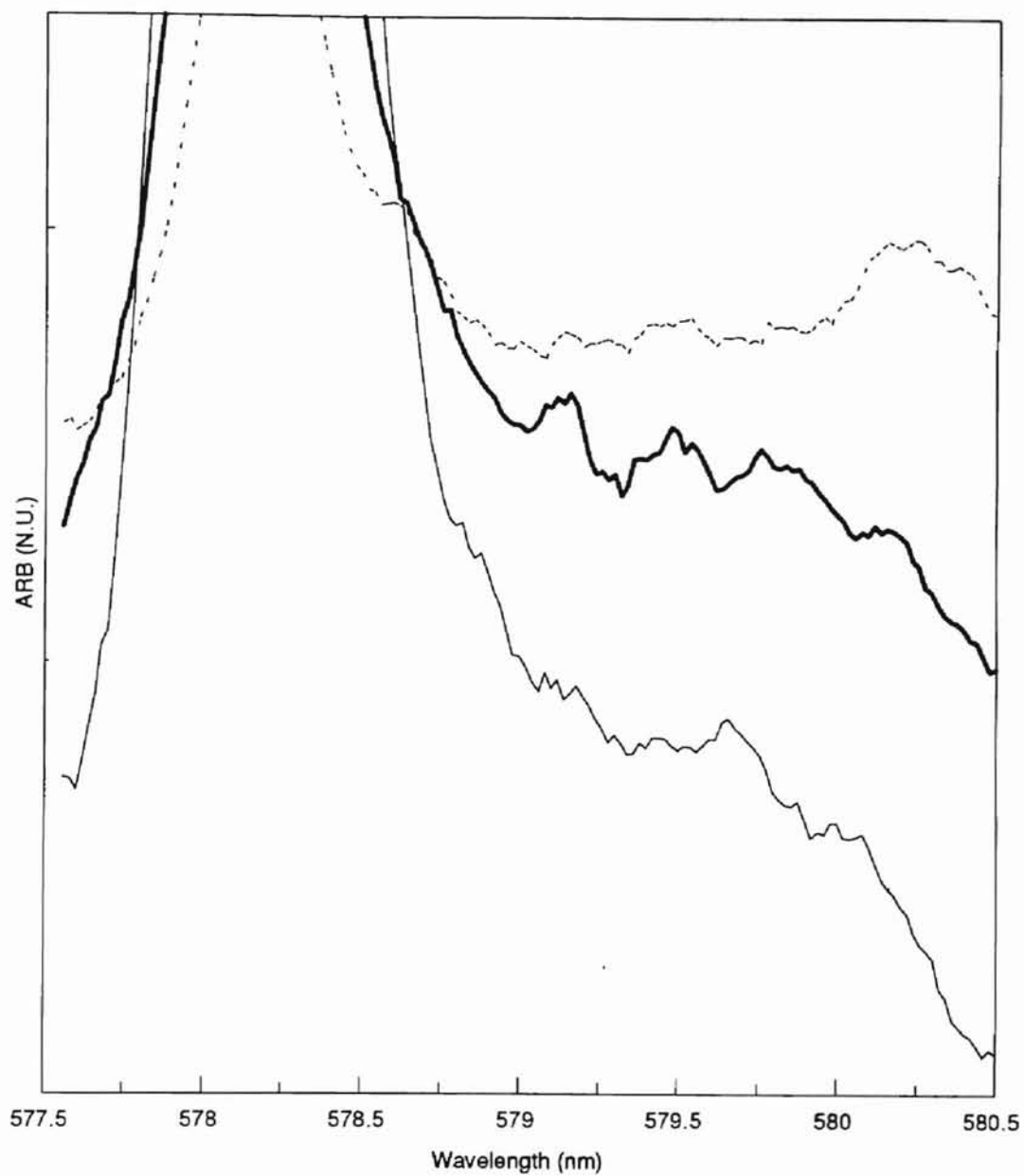


Figure 16: LS glass spectra obtained at an excitation wavelength of $\lambda_{ex} = 578$ nm. This series of graphs were taken at a temperature of 70 K and $T = 1.0, 3.0,$ and 5.0 ms.

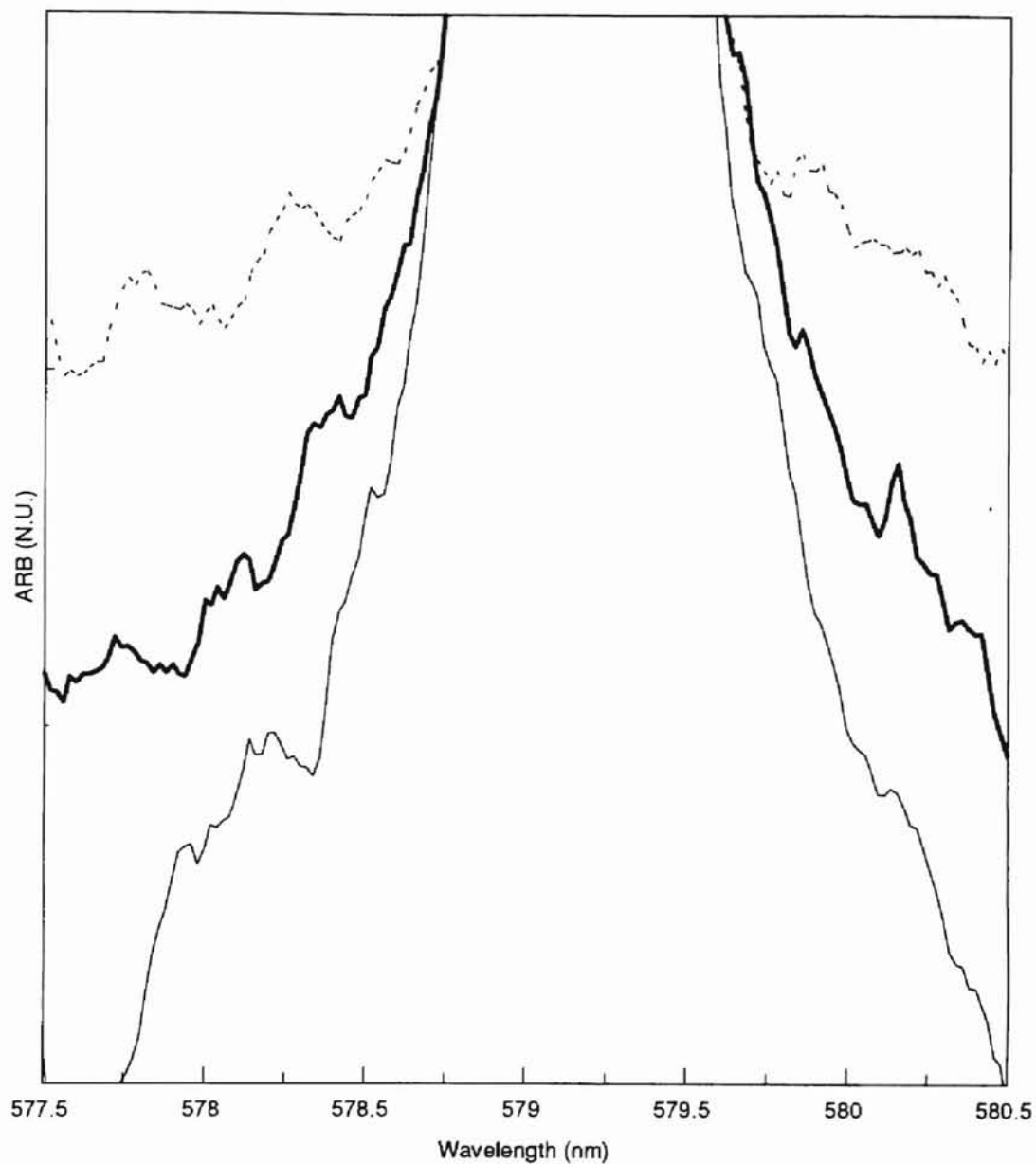


Figure 17: LS glass spectra obtained at an excitation wavelength of $\lambda_{ex} = 579$ nm. This series of graphs were taken at a temperature of 70 K and $T = 1.0, 3.0,$ and 5.0 ms.

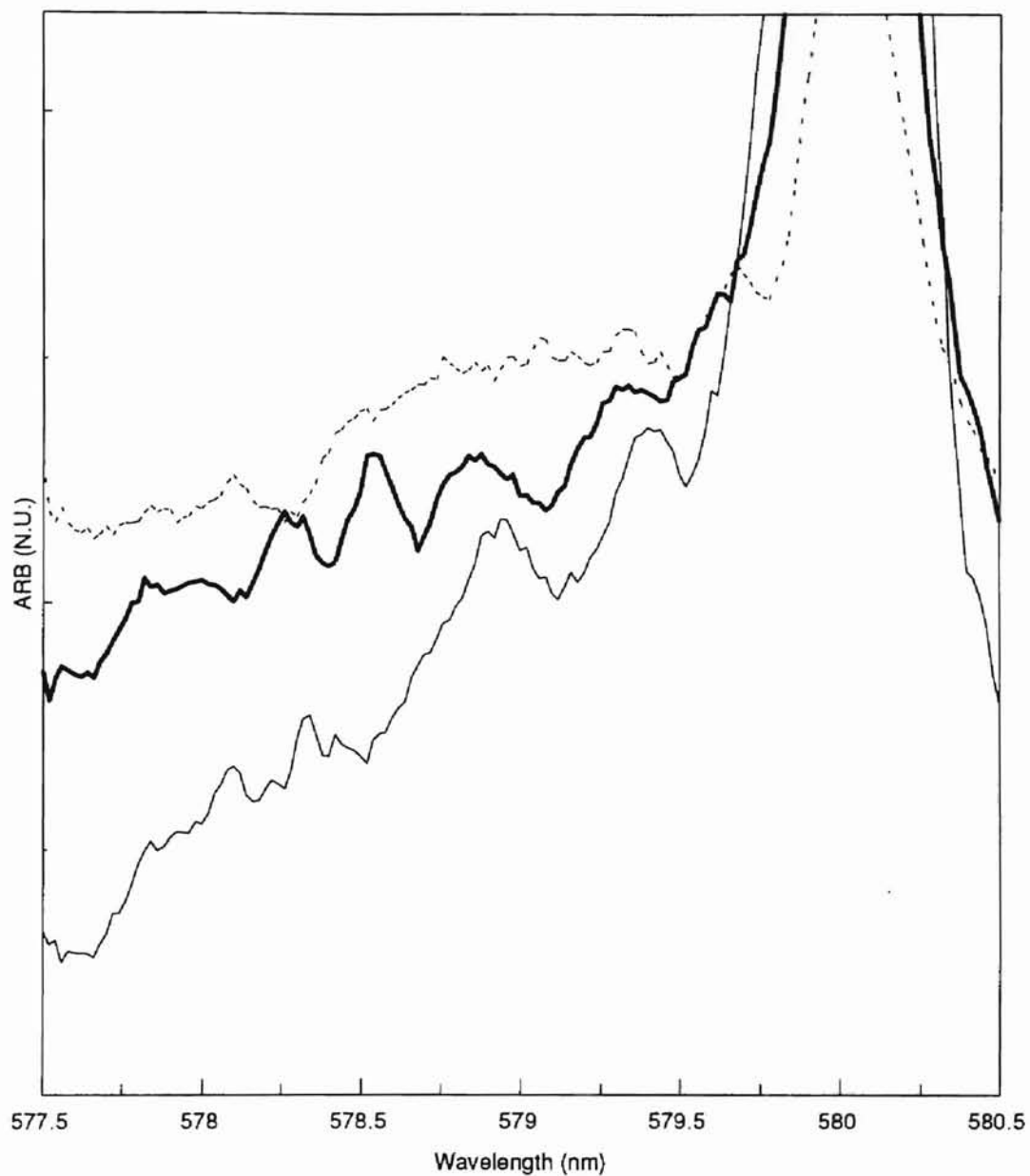


Figure 18: LS glass spectra obtained at an excitation wavelength of $\lambda_x = 580$ nm. This series of graphs were taken at a temperature of 70 K and $T = 1.0, 3.0,$ and 5.0 ms.

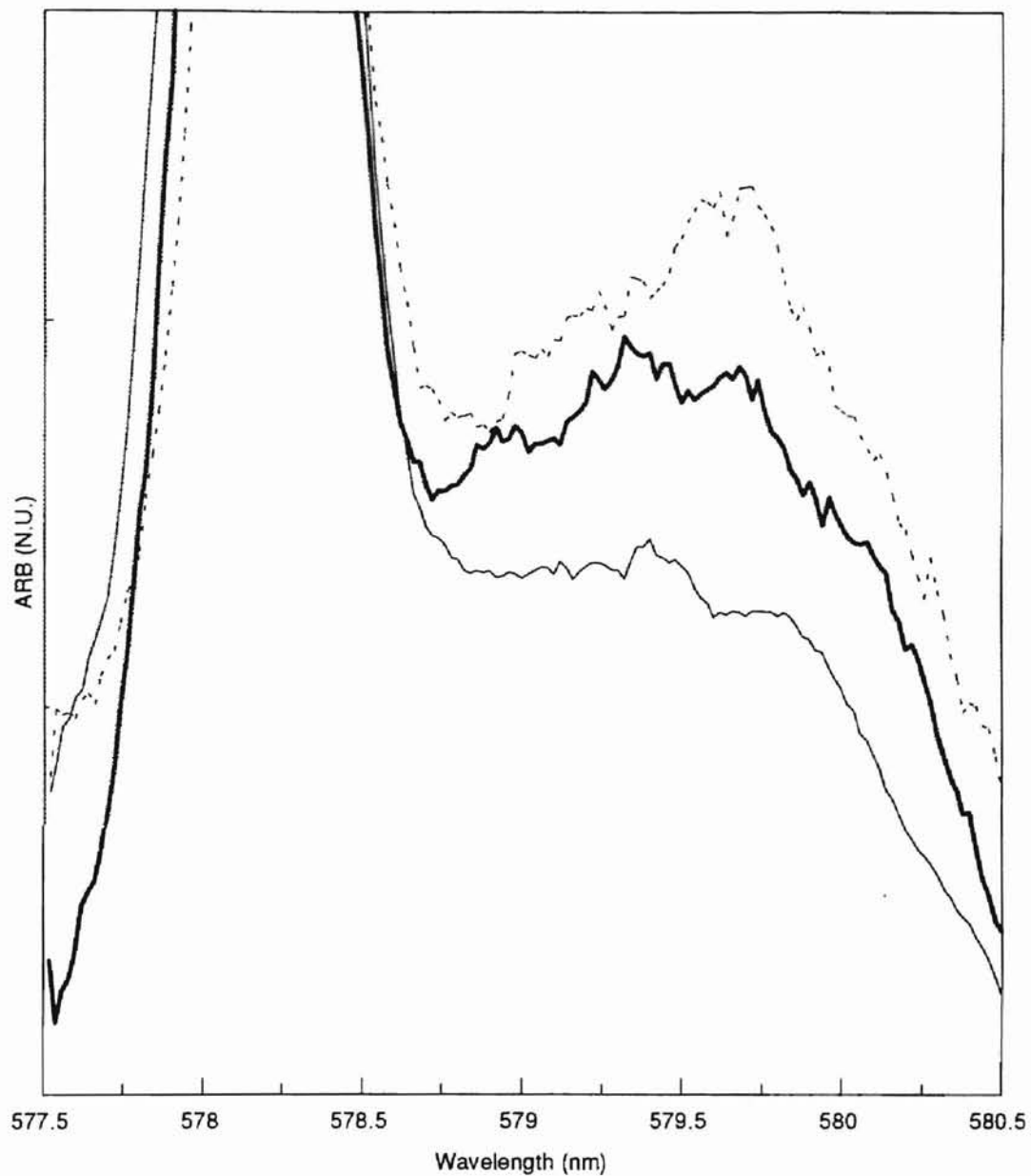


Figure 19: LiSiO glass spectra obtained at an excitation wavelength of $\lambda_{ex} = 578$ nm. This series of graphs were taken at a temperature of 70 K and $T = 1.0, 3.0,$ and 5.0 ms.



Figure 20: LiSiO glass spectra obtained at an excitation wavelength of $\lambda_{ex} = 579$ nm. This series of graphs were taken at a temperature of 70 K and $T = 1.0, 3.0,$ and 5.0 ms.

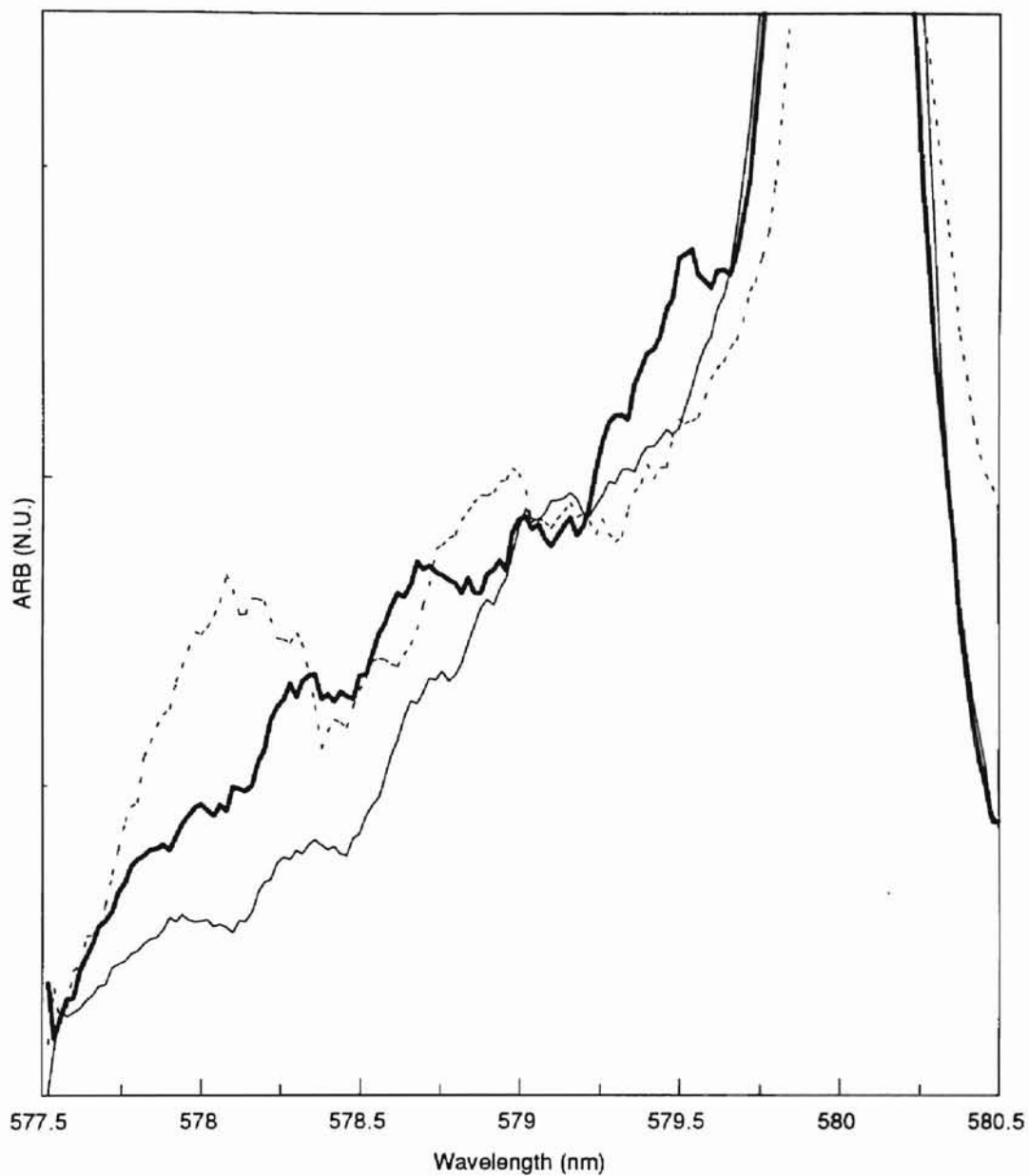


Figure 21: LiSiO glass spectra obtained at an excitation wavelength of $\lambda_x = 580$ nm. This series of graphs were taken at a temperature of 70 K and $T = 1.0, 3.0,$ and 5.0 ms.

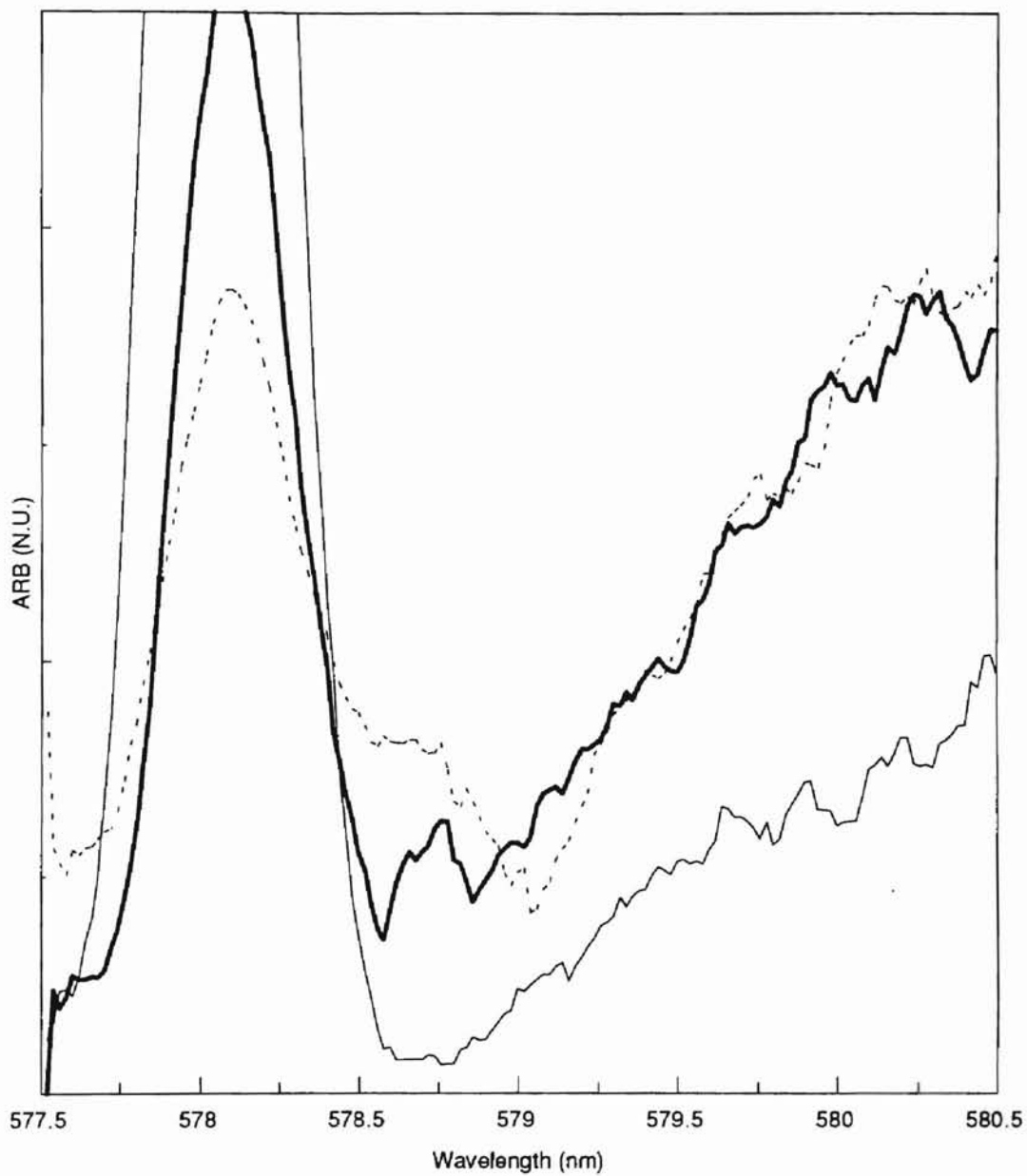


Figure 22: Na glass spectra obtained at an excitation wavelength of $\lambda_{ex} = 578$ nm. This series of graphs were taken at a temperature of 70 K and $T = 1.0, 3.0,$ and 5.0 ms.

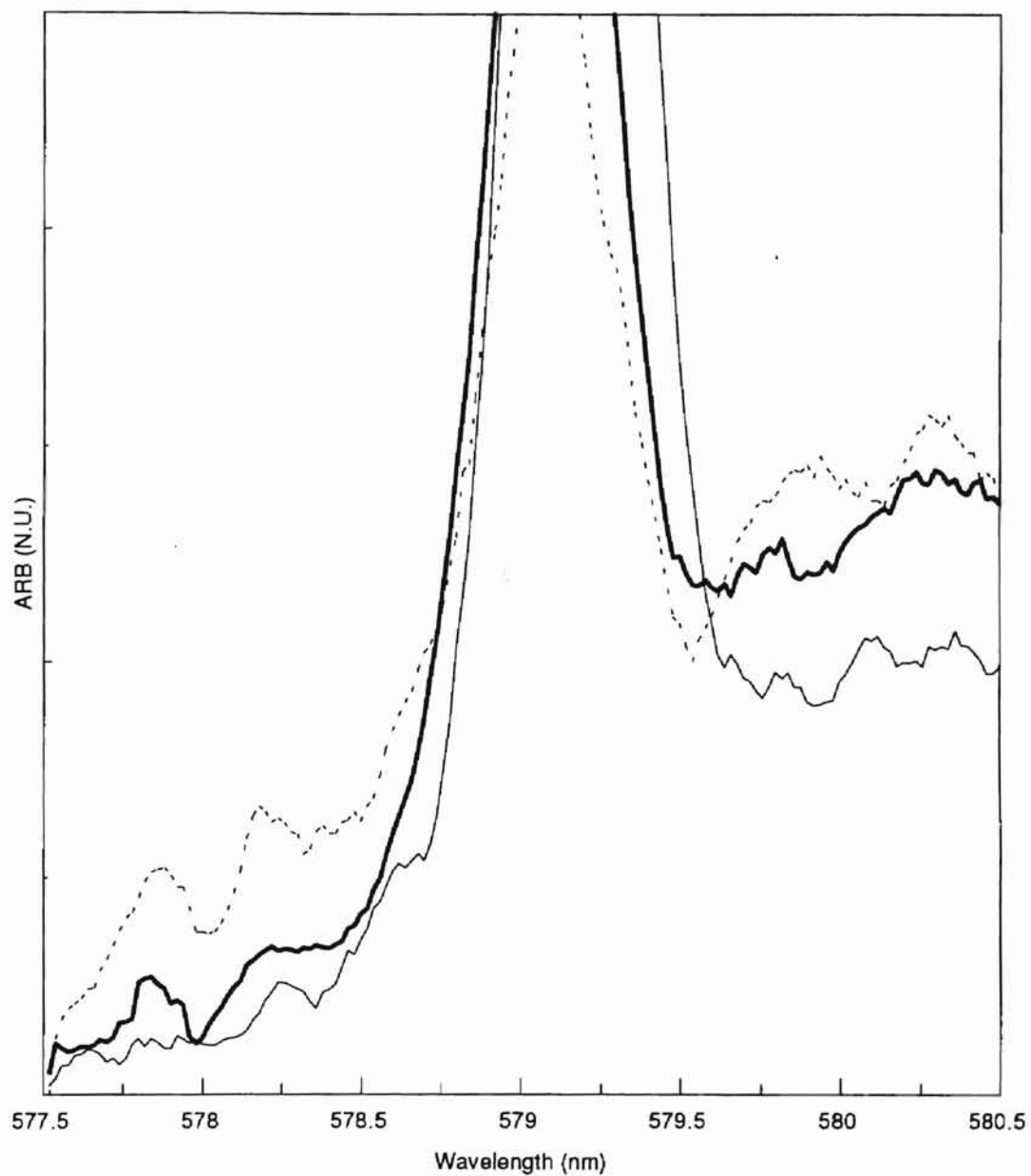


Figure 23: Na glass spectra obtained at an excitation wavelength of $\lambda_x = 579$ nm. This series of graphs were taken at a temperature of 70 K and $T = 1.0, 3.0,$ and 5.0 ms.

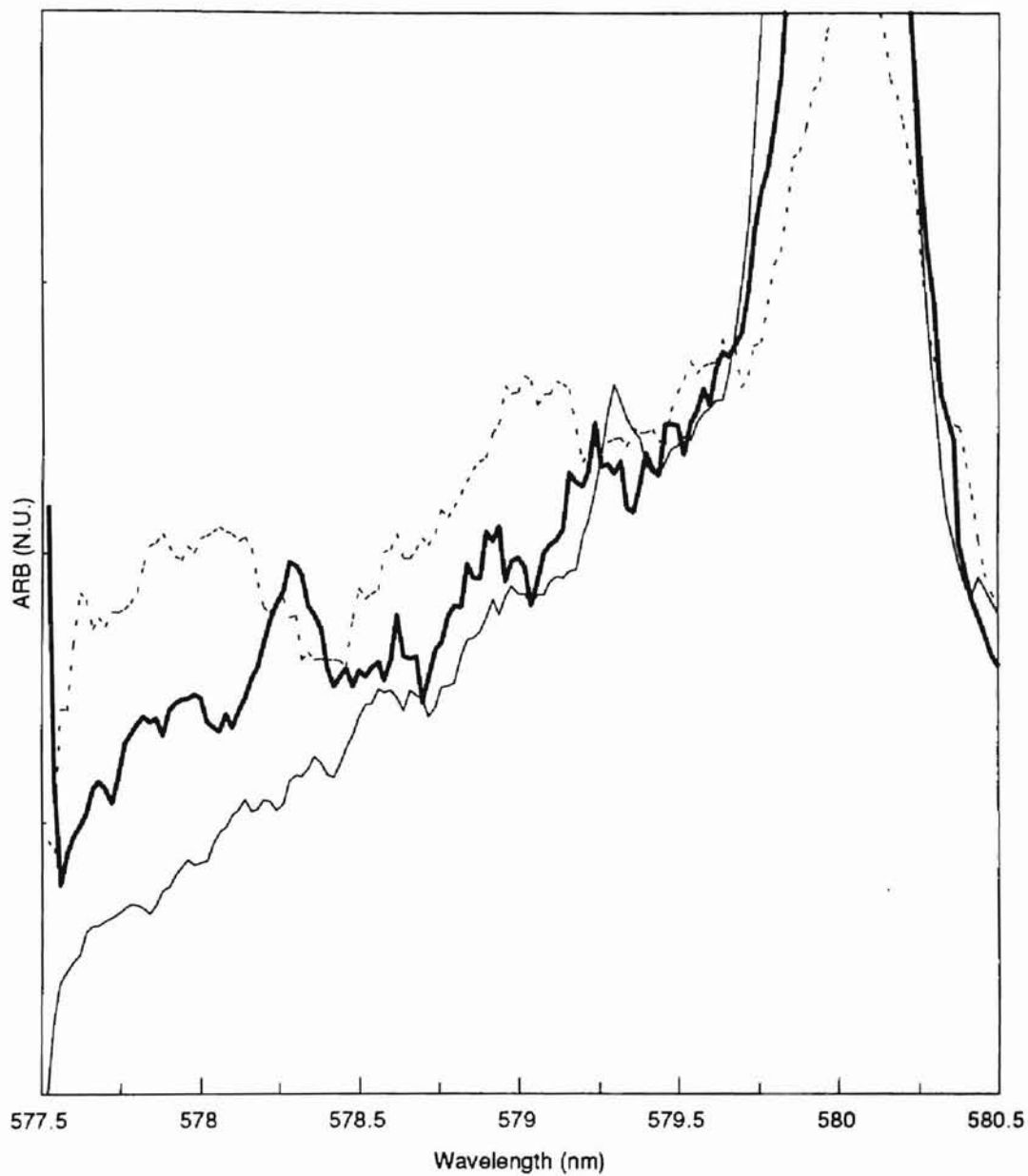


Figure 24: Na glass spectra obtained at an excitation wavelength of $\lambda_x = 580$ nm. This series of graphs were taken at a temperature of 70 K and $T = 1.0, 3.0,$ and 5.0 ms.

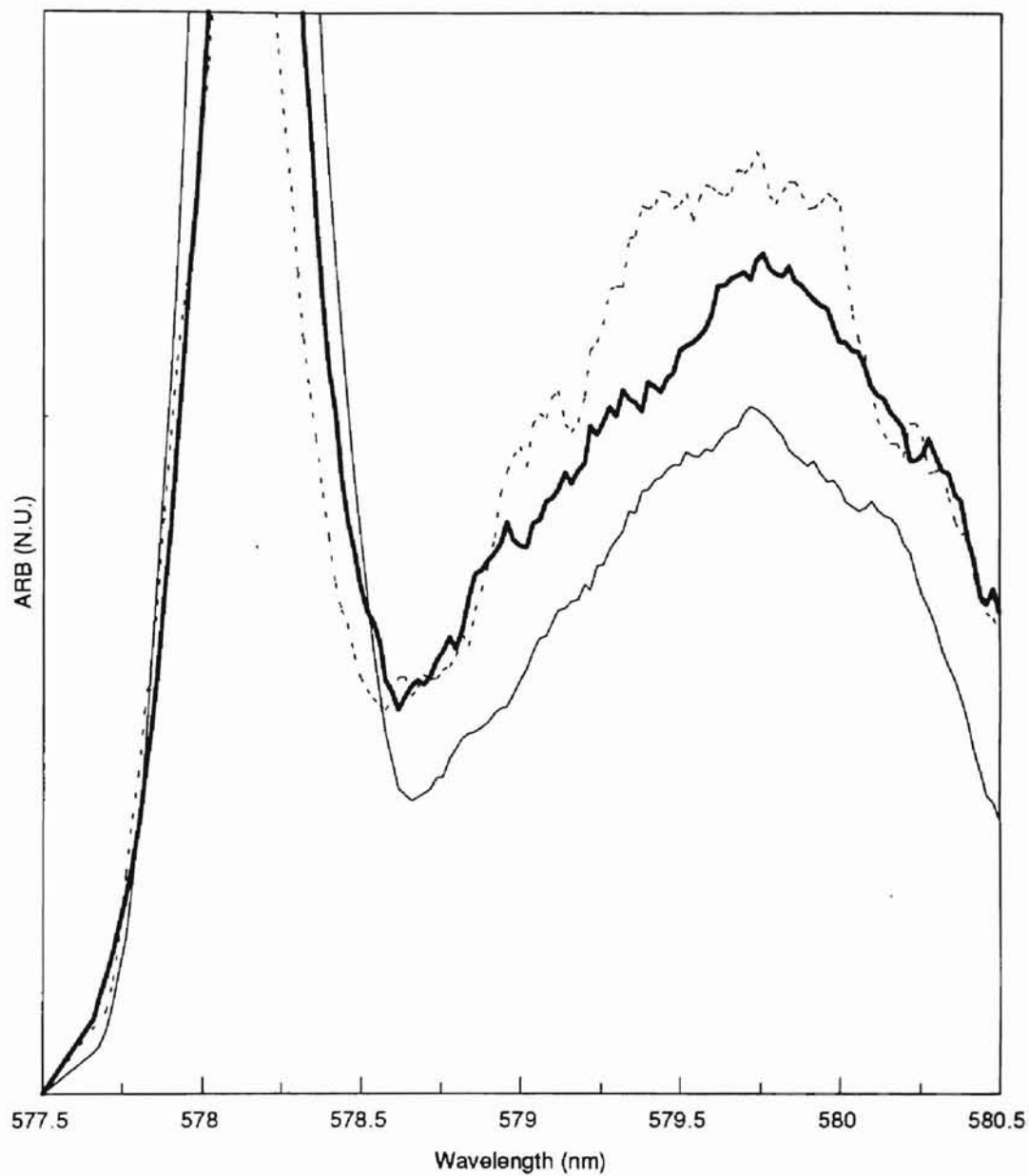


Figure 25: Rb glass spectra obtained at an excitation wavelength of $\lambda_{ex} = 578$ nm. This series of graphs were taken at a temperature of 70 K and $T = 1.0, 3.0,$ and 5.0 ms.

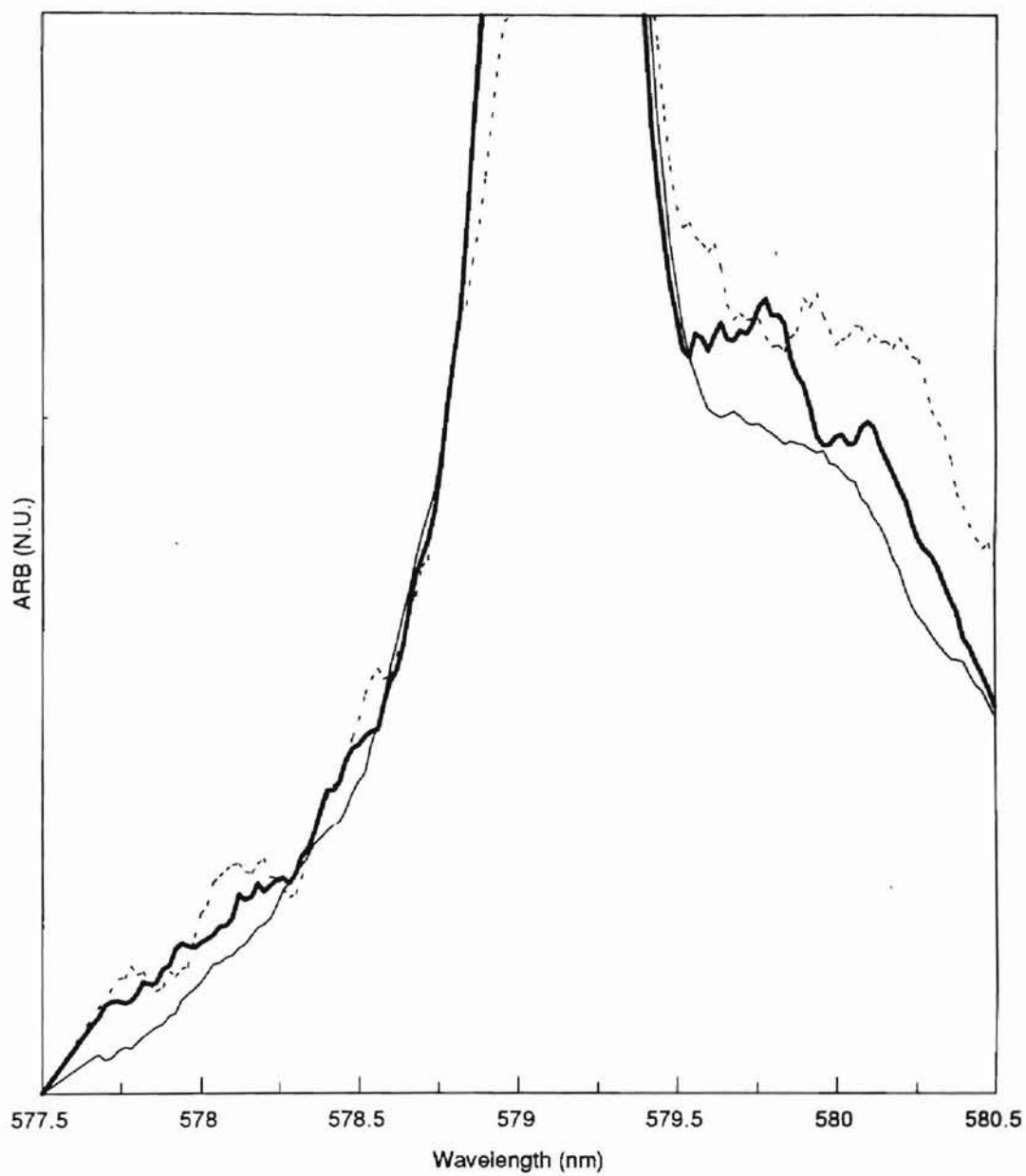


Figure 26: Rb glass spectra obtained at an excitation wavelength of $\lambda_x = 579$ nm. This series of graphs were taken at a temperature of 70 K and $T = 1.0, 3.0,$ and 5.0 ms.

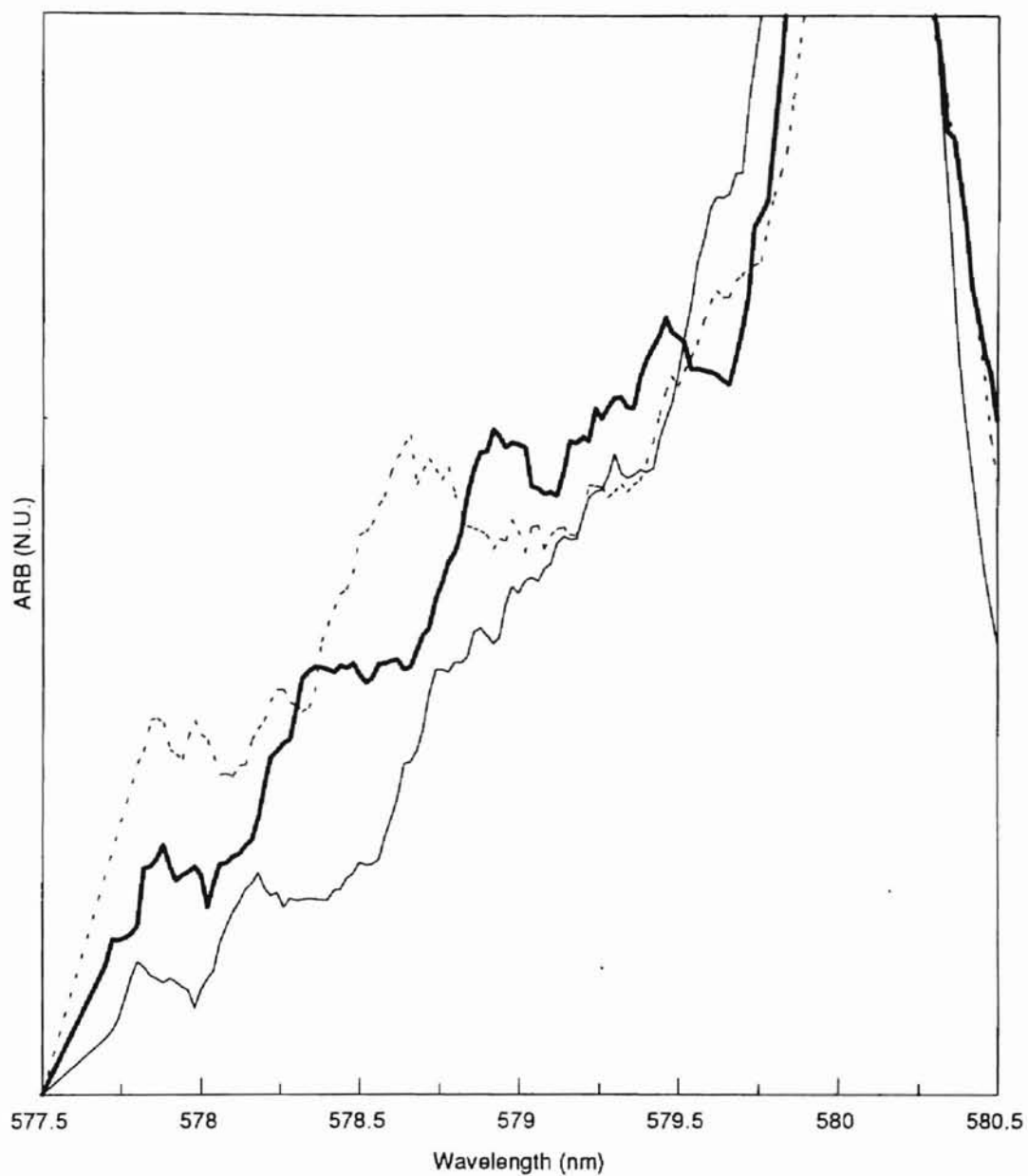


Figure 27: Rb glass spectra obtained at an excitation wavelength of $\lambda_{ex} = 580$ nm. This series of graphs were taken at a temperature of 70 K and $T = 1.0, 3.0,$ and 5.0 ms.

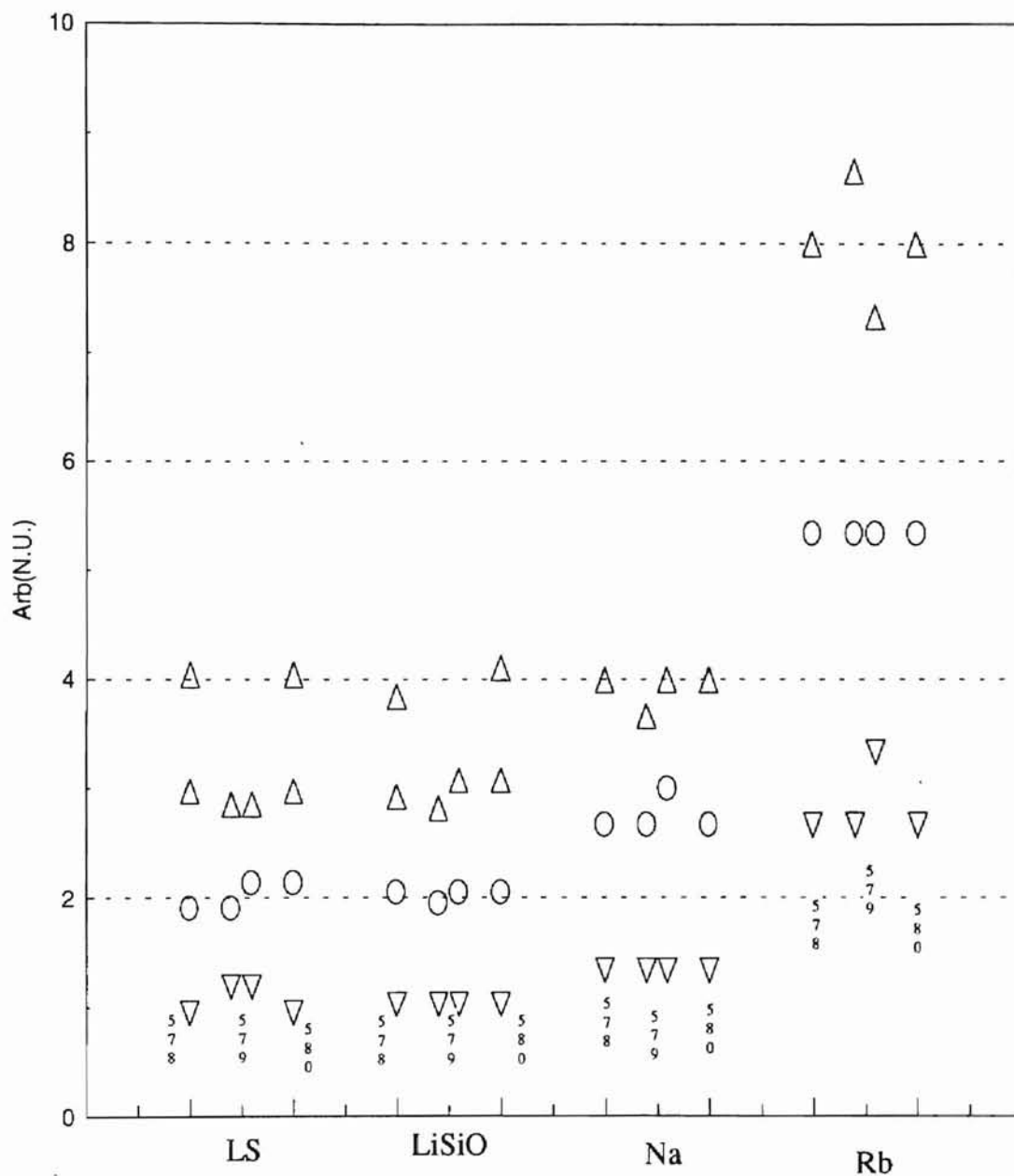


Figure 28: Plot of the onset of side peaks using their respective mobility edges as the scaling factor. The glasses are in this order LS, LiSiO, Na, and Rb with 578, 579(anti-stokes), 579(stokes), and 580 nm respectively.

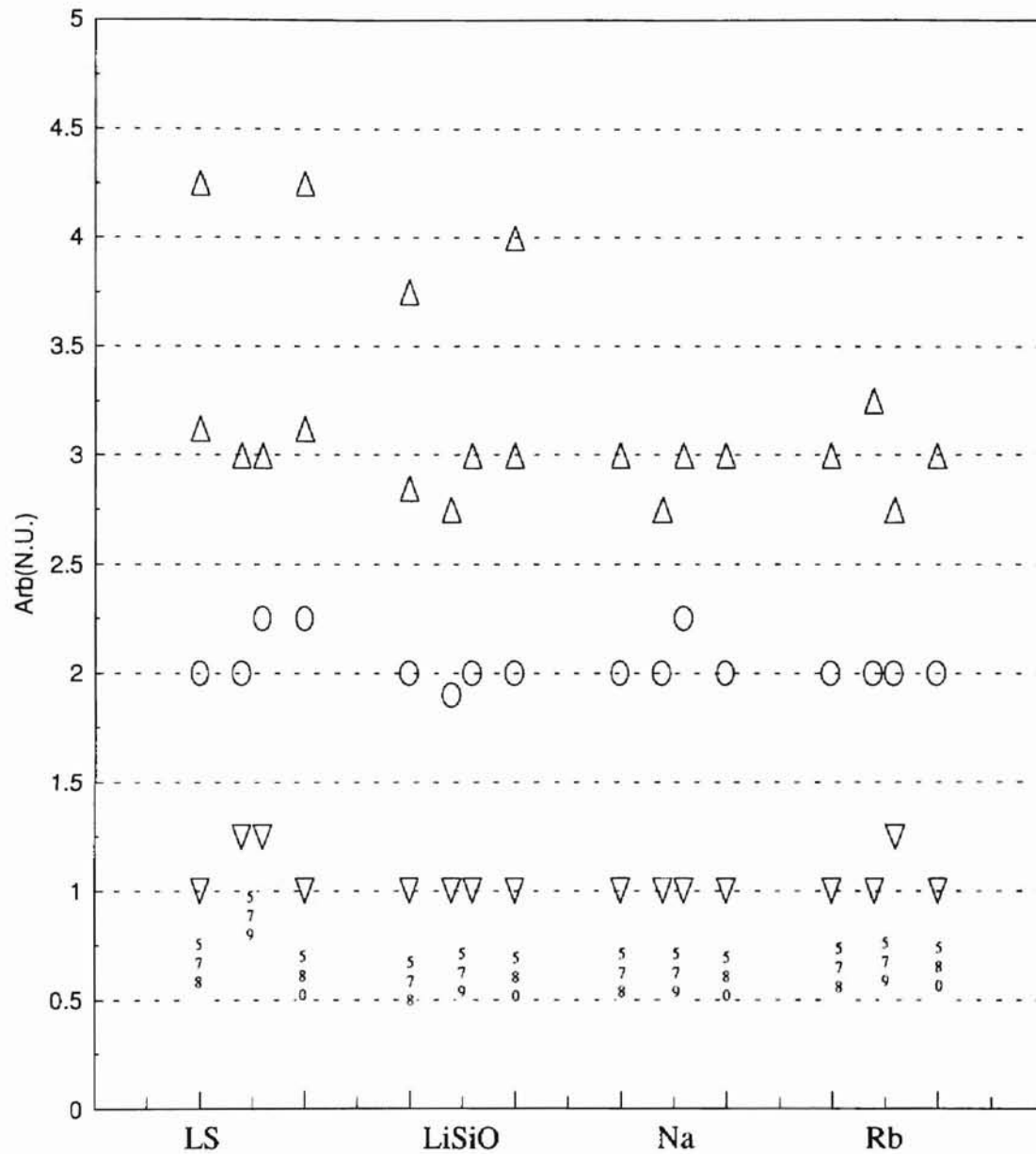


Figure 29: Plot of the onset of side peaks normalized with respect to their lowest peak value. The glasses are in this order LiSiO, Na, and Rb with 578, 579 (anti-stokes), 579 (stokes), and 580 nm respectively.

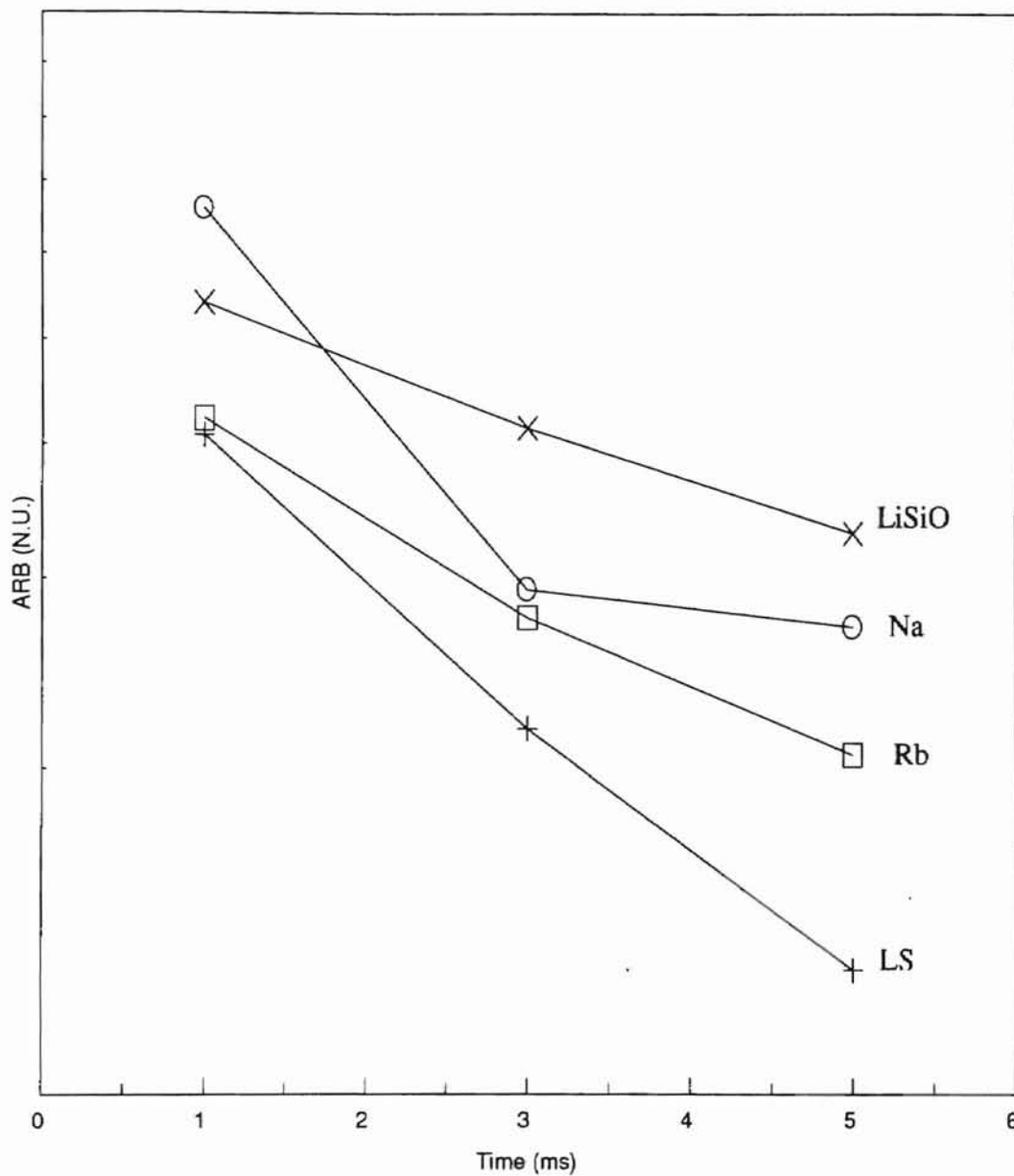


Figure 30: Spectral Peak Area vs. Time log plot for an excitation of 578 nm at 70 K, ranging from $T= 1.0, 3.0,$ and 5.0 ms for LS, LiSiO, Na, and Rb glasses. Demonstrating a constant decline in the area under the curve.

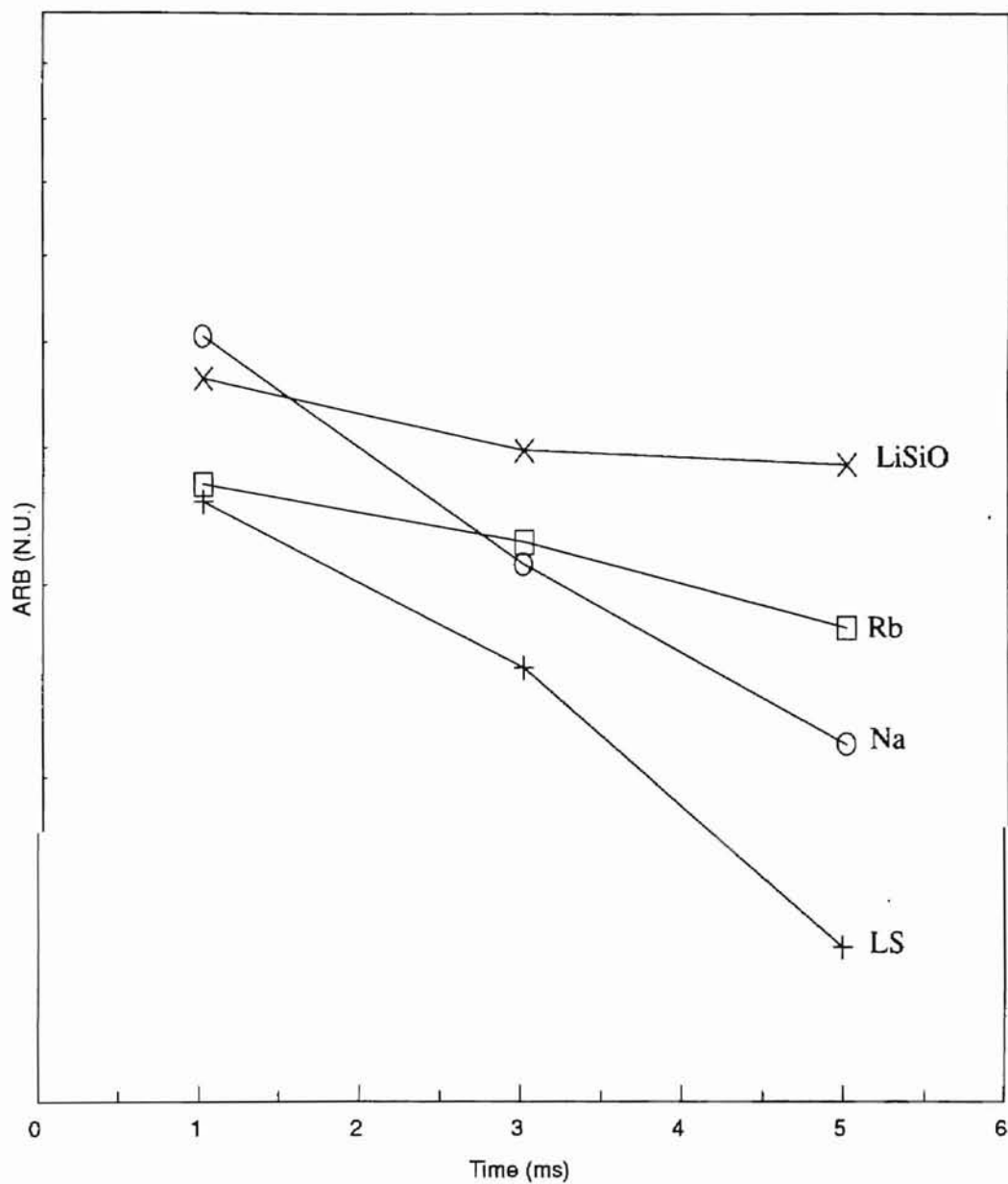


Figure 31: Spectral Peak Area vs. Time log plot for an excitation of 579 nm at 70 K, ranging from $T=1.0, 3.0,$ and 5.0 ms for LS, LiSiO, Na, and Rb glasses. Demonstrating a constant decline in the area under the curve.

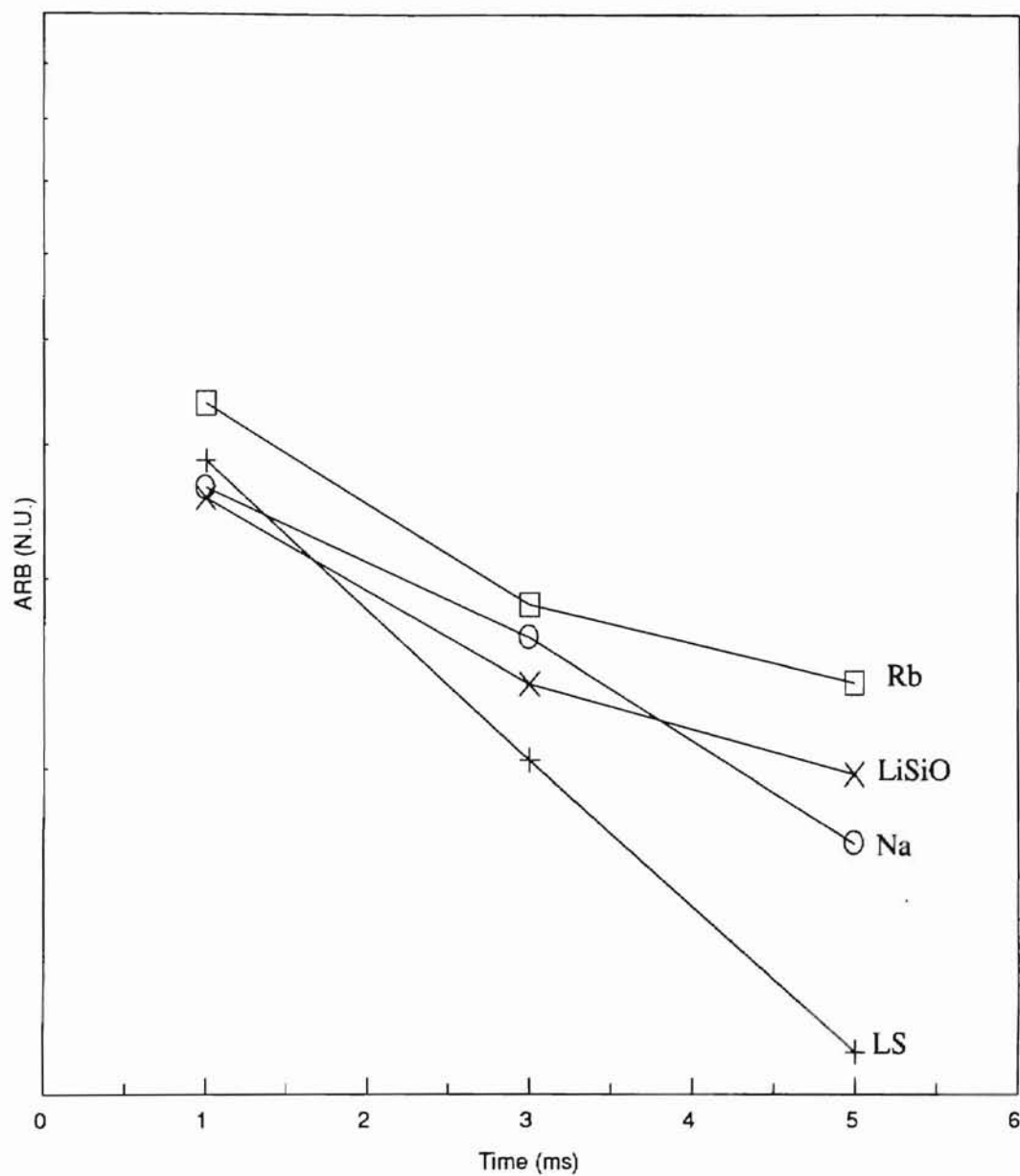


Figure 32: Spectral Peak Area vs. Time log plot for an excitation of 580 nm at 70 K, ranging from $T= 1.0, 3.0, \text{ and } 5.0$ ms for LS, LiSiO, Na, and Rb glasses. Demonstrating a constant decline in the area under the curve.

Energy Transfer Characteristics

FLN has provided valuable information to support the model that phonons near the mobility edge enhance the energy transfer from the Eu^{3+} ions. A method has been developed by Brawer and Weber [20] to characterize quantitative energy transfer between ions in different types of sites. The glass spectra were analyzed to determine an average ion-ion transfer time, using this relation:

$$I(\omega, t) = a(t)I(\omega, 0) + [1 - a(t)]I(\omega, \infty), \quad (7)$$

where $I(\omega, t)$, is normalized for unit area:

$$\int_0^{\infty} I(\omega, t) d\omega = 1. \quad (8)$$

The spectral energy transfer time is given as:

$$a(t) = \frac{\int_{\omega_1}^{\omega_2} [I(\omega, t) - I(\omega, \infty)] d\omega}{\int_{\omega_1}^{\omega_2} [I(\omega, 0) - I(\omega, \infty)] d\omega}. \quad (9)$$

In equation (9), the integral was approximated as a summation over the entire curve. $I(\omega, t)$ was taken as the varying intensities of the different time intervals after

the excitation pulse. $I(\omega, \infty)$ for all these curves were approximated to zero to simplify the calculations. $I(\omega, 0)$ was taken to be the intensity at our base scan of 1.0 ms for each set of curves [20]. The results of these calculations can be seen in Table IV.

The spectral energy coefficient $a(t)$, figures 35 - 38, all exhibit exponential like declines in there. As seem in Table IV the spectral energy coefficient does not follow the expected order of the periodic table. Instead, Na has the fastest spectral energy coefficient over Rb which was expected to be the fastest. While the LS glasses have a more gradual decline, that might be attributed to the Eu^{3+} concentration. The LS glass that contains only 3.0% has the slowest spectral energy coefficient.

TABLE IV

SPECTRAL ENERGY COEFFICIENT $a(t)$

Time (ms)	LS Glass $a(t)$	LiSiO Glass $a(t)$	Na Glass $a(t)$	Rb Glass $a(t)$
Wavelength 578 nm				
1.0 ms	1.0	1.0	1.0	1.0
3.0 ms	0.85302	0.85008	0.46985	0.66213
5.0 ms	0.83823	0.74638	0.35242	0.58746
Wavelength (nm) 579 nm				
1.0 ms	1.0	1.0	1.0	1.0
3.0 ms	0.94024	0.89041	0.86836	0.90870
5.0 ms	0.92782	0.85469	0.68368	0.75457
Wavelength (nm) 580 nm				
1.0 ms	1.0	1.0	1.0	1.0
3.0 ms	0.92984	0.81434	0.79663	0.76748
5.0 ms	0.90117	0.68598	0.56427	0.67071

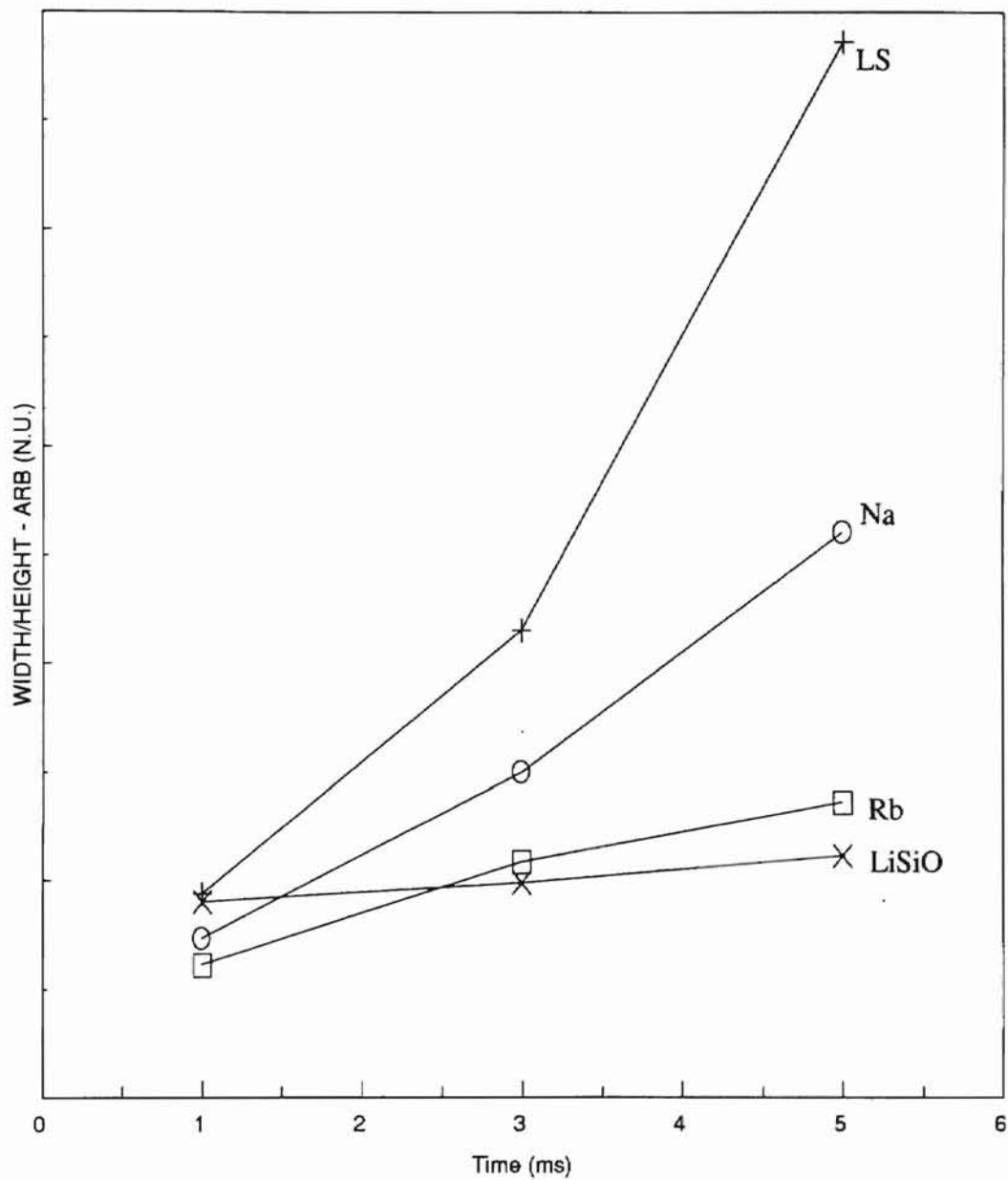


Figure 33: Normalized Width vs. Time plot for an excitation of 578 nm at 70 K, ranging from $T= 1.0, 3.0,$ and 5.0 ms for LS, LiSiO, Na, and Rb glasses.

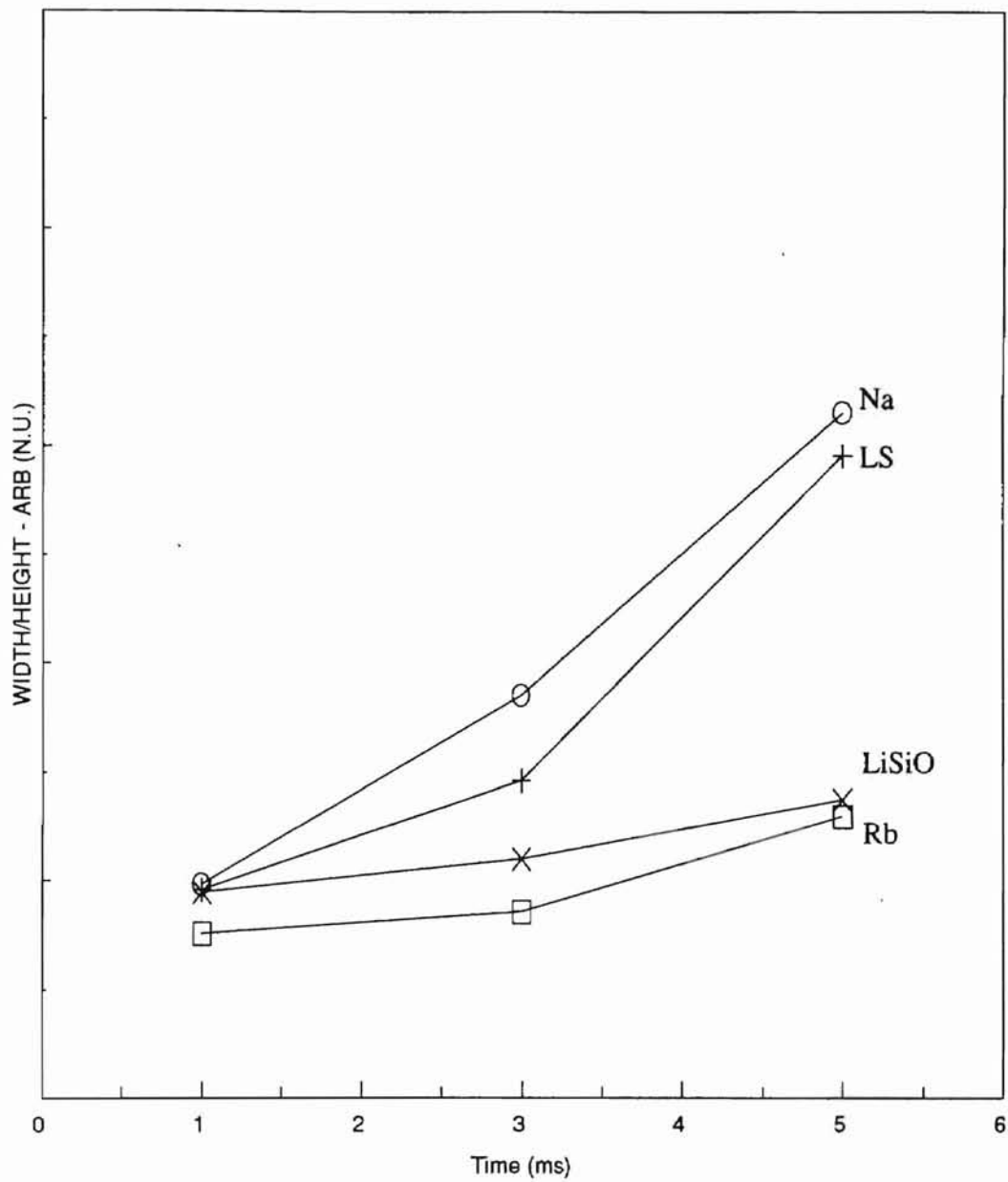


Figure 34: Normalized Width vs. Time plot for an excitation of 579 nm at 70 K, ranging from $T= 1.0, 3.0,$ and 5.0 ms for LS, LiSiO, Na, and Rb glasses.

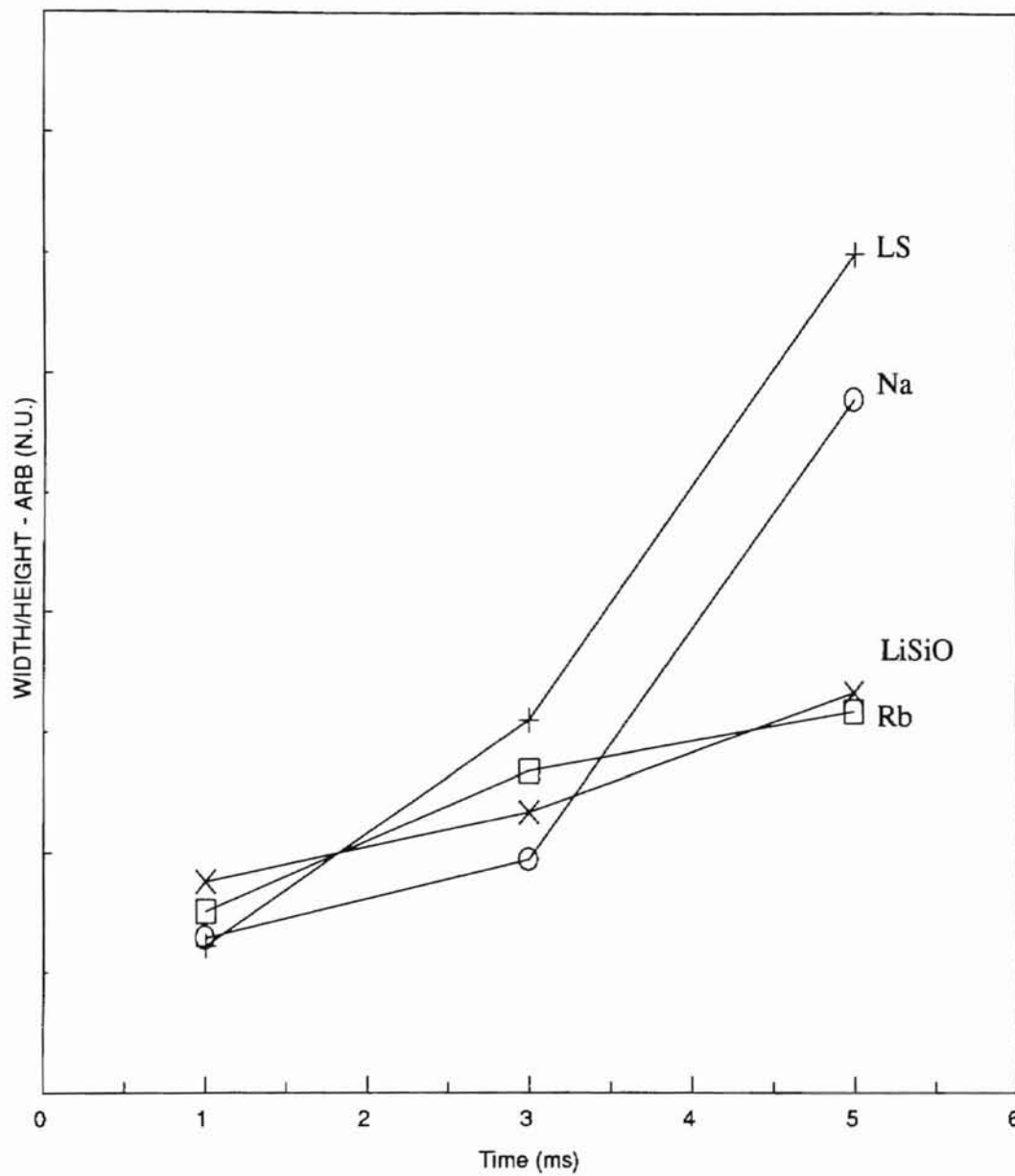


Figure 35: Normalized Width vs. Time plot for an excitation of 580 nm at 70 K, ranging from $T=1.0, 3.0,$ and 5.0 ms for LS, LiSiO, Na, and Rb glasses.

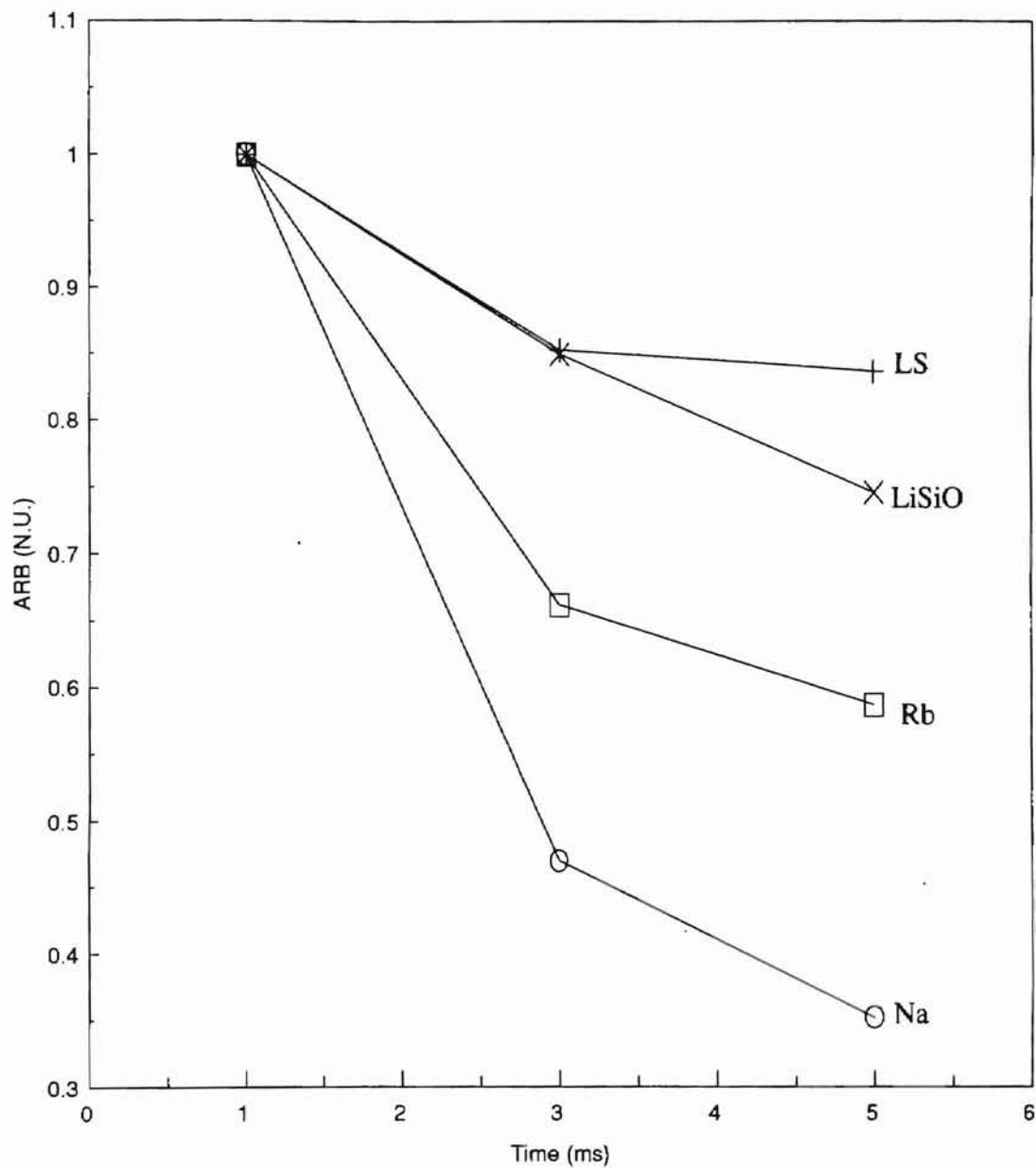


Figure 36: Spectral Energy Transfer vs. Time plot for an excitation of 578 nm at 70 K, ranging from $T=1.0, 3.0,$ and 5.0 ms for LS, LiSiO, Na, and Rb glasses.

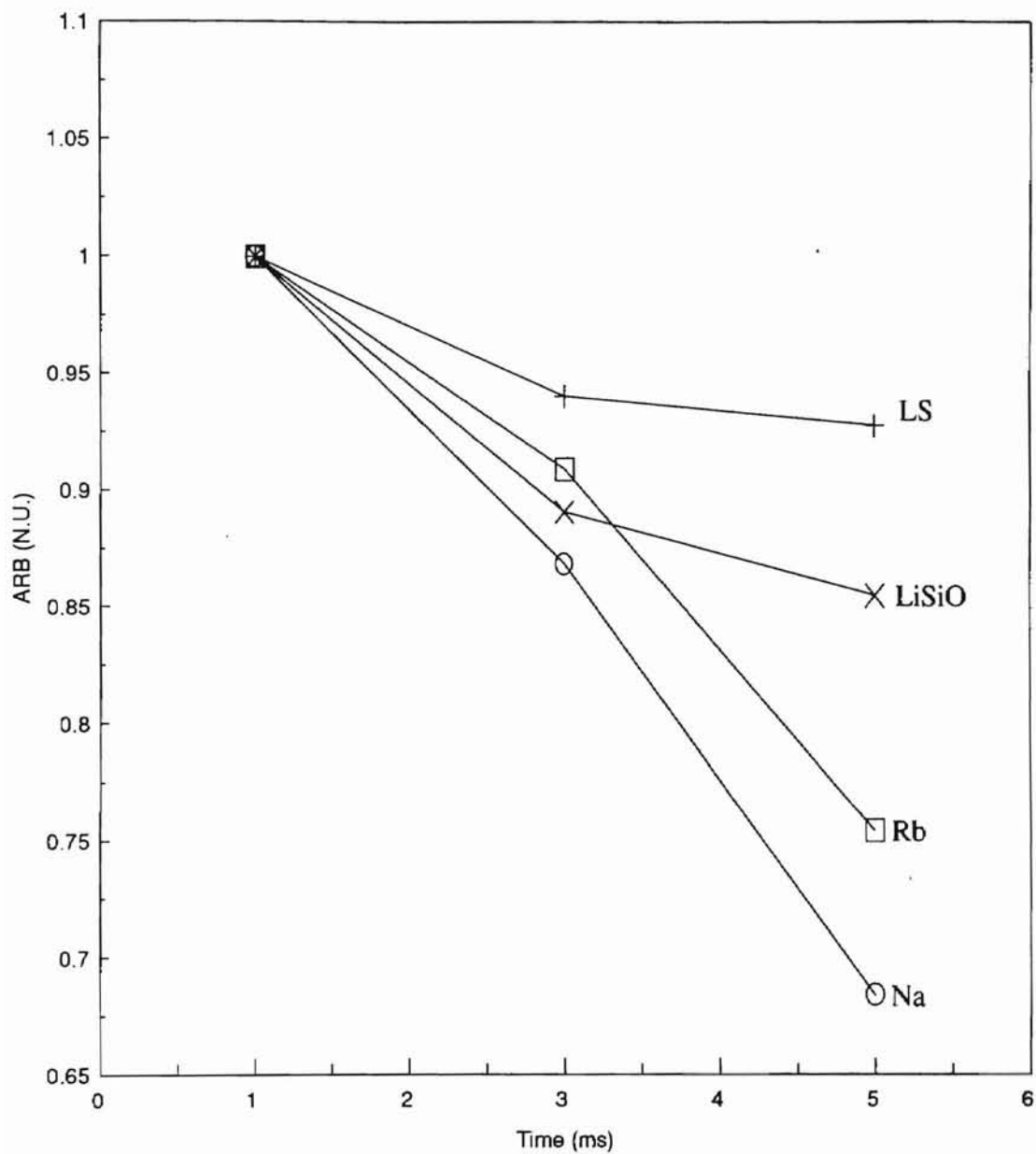


Figure 37: Spectral Energy Transfer vs. Time plot for an excitation of 579 nm at 70 K, ranging from $T=1.0, 3.0,$ and 5.0 ms for LS, LiSiO, Na, and Rb glasses.

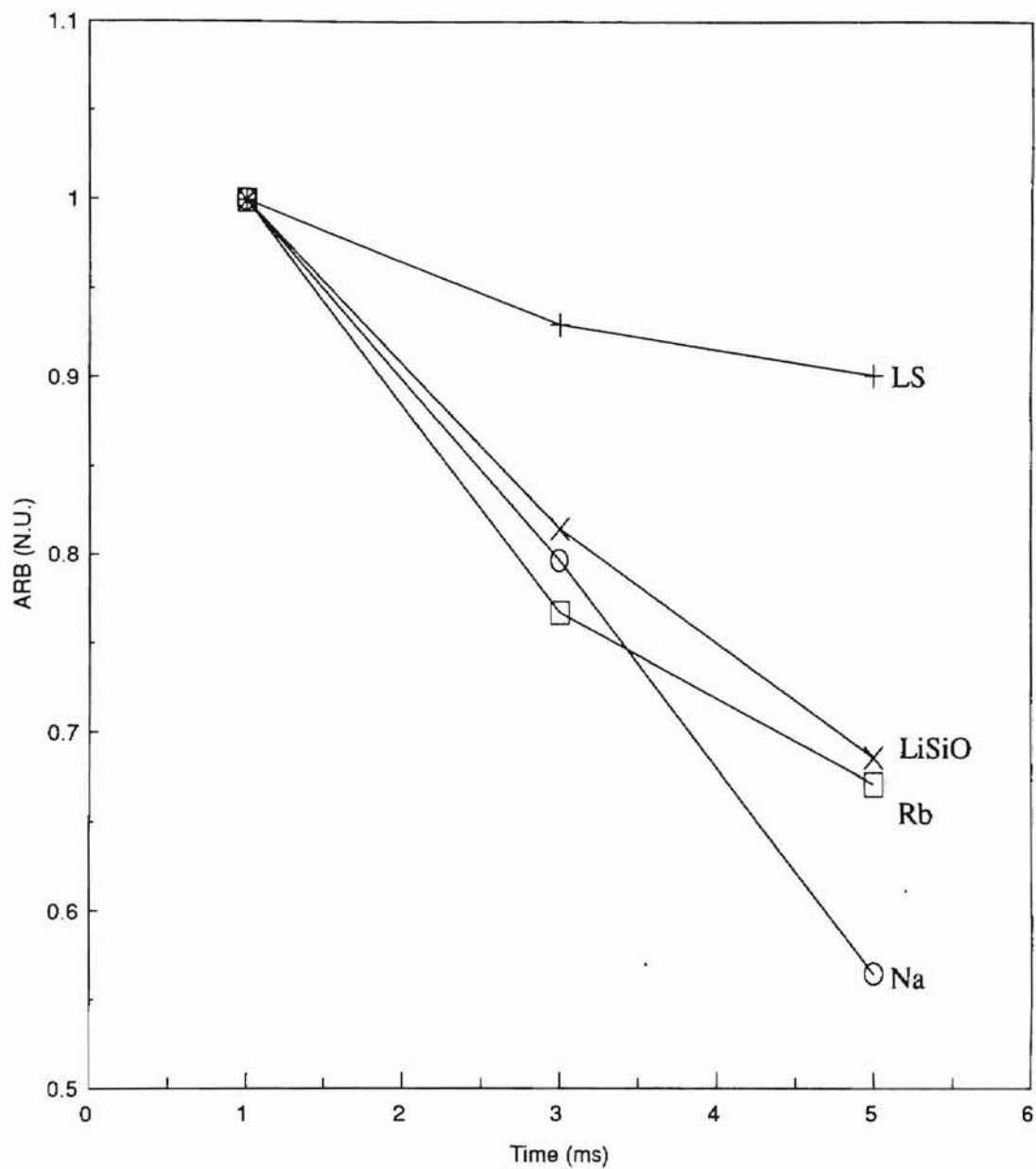


Figure 38: Spectral Energy Transfer vs. Time plot for an excitation of 580 nm at 70 K, ranging from $T= 1.0, 3.0,$ and 5.0 ms for LS, LiSiO, Na, and Rb glasses.

CHAPTER IV

SUMMARY AND CONCLUSION

Time-resolved site-selection spectroscopy techniques have been used in the examination of four glasses doped with Eu^{3+} ions. These four glasses are composed of $0.15(\text{M}_2\text{O})0.05(\text{ZnO})0.05(\text{BaO})0.05(\text{Eu}_2\text{O}_3)0.70(\text{SiO}_2)$, where the M is Li, Na, or Rb. Glasses in this family all contain 5.0% Eu^{3+} ions except the control glass, which has 3.0%. The use of the lowest-frequency Raman peak has been used as a quantitative measure of the mobility edge. In this examination, the mobility edge has been taken to represent the onset of localized phonons. Absorption spectra were also taken to determine regions of high concentrations of Europium. These absorption spectra were also used in the analysis of the FLN fluorescence spectrums.

The analysis of the FLN (see figures 16 - 27) spectra described in this paper explains the appearance of side peaks in the spectral graphs as enhanced energy transfer mediated by localized phonons. All the glasses in this study adhere the Dixon model, but only the two LS glasses demonstrate that a particular phonon mediates the enhanced energy transfer. The fluorescence spectra of the LS glasses correspond to the leading edge of the boson peak that indicates areas of enhanced energy transfer. On the other hand, the leading edge might correspond to a different particular phonon

that is significant to energy transfer. A fascinating phenomenon noticed in all the glasses' FLN fluorescence spectra was a common spacing of 0.4 THz. This can be explained in one or two ways: either the mobility edges for these glasses are incorrectly calculated or the 0.4 THz spacing is due to a type of localized phonon that has been caused by the clustering of the Eu^{3+} ions.

REFERENCES

1. R. Reisfeld, in: *Spectroscopy of Solid-State Laser-Type Material*, (Plenum Press, New York, 1987) p. 343.
2. X. Gang, G. Boulon, and R. C. Powell, *J. Chem. Phys.*, **78**(7), 4374(1983).
3. X. Gang, and R. C. Powell, *J. Appl. Phys.*, **57** (4) 1229(1985).
4. J. Hegarty, W. M. Yen; and M. J. Weber, *Phys. Rev.*, **B**(18), 5816(1978).
5. M. J. Weber, in: *Laser Spectroscopy of Solids*, eds.: W. M. Yen and P. M. Selzer (Springer, New York, 1981) p.189.
6. L. A. Riesberg, *Phys. Rev. A*(9), 671(1975).
7. J. D. Cutnell, and Kenneth W. Johnson, *Physics*, John Wiley's Sons(New York 1989) p.790-793.
8. J. Wang, W. S. Brocklesby, J. R. Lincoln, J. E. Townsend, and D. N. Payne, *J. Non-Crystalline Solids*, 163(1993).
9. F. L. Galeener, in: Kinser, *Effects of Modes of Formation on the Structure of Glasses*, Trans Tech Publications Ltd, Switzerland, 1987, p.310.
10. C. Kittel, *Introduction to Solid State* (6th editon), John Wiley & Son 1986.
11. R. Zallen, in: *The Physics of Amorphous Solids*, John Wiley & Sons, Inc., (New York, 1983).
12. C. R. A. Catlow, in: *Defects and Disorders in Crystalline and Amorphous Solids*, Series C: Mathematical and Physical Sciences, **418** ed. C. R. A. Catlow, Kluwer Academic Publishers, 1991.
13. G. F., Imbusch, and R., Kopelman, in: *Laser Spectroscopy of Solids*, eds. W. M. Yen and P. M. Selzer, (Springer, New York, 1981) p. 18.

14. T. Holstein, S. K. Lyo, and R. Orbach, in: *Laser Spectroscopy of Solids*, eds. W. M. Yen and P. M. Selzer, (Springer, New York, 1981) p. 39.
15. G. S. Dixon, *Journal of Luminescence*, **45**, (1990) 93-95.
16. C. Brecher, and L. A. Riseberg, *J. Appl. Phys.*, **57**, 4, 1985.
17. G. S. Dixon, B. D. Gault, S. Shi, P. A. Watson, and J. A. Wicksted, *Phys. Rev.* **B(49)**, 1 1994.
18. B. Golding, J. E. Graebner, and L. C. Allen, in: *Phonon Scattering Condensed Matter V*, eds. A. C. Anderson and J. P. Wolfe (Springer, Berlin, 1986) p. 23.
19. U. Buchenau, M. Prager, N. Nueker, A. J. Dianoux, N. Ahmad, and W. A. Phillips, *Phys. Rev.*, **B(34)**, 5666(1986) .
20. S. A. Brawer, and M. J. Weber, *Appl. Phys. Lett.*, **35**(1), 1(1979).

VITA

Michael Dewayne Furlough

Candidate for the Degree of

Master of Science

Thesis: ENERGY TRANSFER IN Eu^{3+} DOPED GLASSES

Major Field: Physics

Biographical:

Personal Data: Born in Little Rock, Arkansas, on August 21, 1969, son of Huskin and Mary Furlough.

Education: Graduated from Little Rock Central High School, Little Rock, Arkansas, in May of 1988. Received the Bachelor of Science degree in Physics with a minor in Mathematics from Dillard University, New Orleans, Louisiana in May of 1992. Completed the requirements for the Master of Science in Physics from Oklahoma State University in July 1996.

Professional Experience: Graduate Teaching Assistant, Oklahoma State University, August 1992 to May 1993. Graduate Research Assistant, Oklahoma State University, May 1993 to present.